© 2023. Published by The Company of Biologists Ltd | Journal of Experimental Biology (2023) 226, jeb246423. doi:10.1242/jeb.246423

RESEARCH ARTICLE

Multiple axes of visual system diversity in Ithomiini, an ecologically diverse tribe of mimetic butterflies

J. Benito Wainwright[1,*], Corin Schofield[1], Max Conway[1], Daniel Phillips[1], Elizabeth Martin-Silverstone[2], Emelie A. Brodrick[3], Francesco Cicconardi[1], Martin J. How[1], Nicholas W. Roberts[1] and Stephen H. Montgomery[1,*]

ABSTRACT

The striking structural variation seen in arthropod visual systems can be explained by the overall quantity and spatio-temporal structure of light within habitats coupled with developmental and physiological constraints. However, little is currently known about how fine-scale variation in visual structures arises across shorter evolutionary and ecological scales. In this study, we characterise patterns of interspecific (between species), intraspecific (between sexes) and intraindividual (between eye regions) variation in the visual system of four ithomiine butterfly species. These species are part of a diverse 26-million-year-old Neotropical radiation where changes in mimetic colouration are associated with fine-scale shifts in ecology, such as microhabitat preference. Using a combination of selection analyses on visual opsin sequences, *in vivo* ophthalmoscopy, micro-computed tomography (micro-CT), immunohistochemistry, confocal microscopy and neural tracing, we quantify and describe physiological, anatomical and molecular traits involved in visual processing. Using these data, we provide evidence of substantial variation within the visual systems of Ithomiini, including: (i) relaxed selection on visual opsins, perhaps mediated by habitat preference, (ii) interspecific shifts in visual system physiology and anatomy, and (iii) extensive sexual dimorphism, including the complete absence of a butterfly-specific optic neuropil in the males of some species. We conclude that considerable visual system variation can exist within diverse insect radiations, hinting at the evolutionary lability of these systems to rapidly develop specialisations to distinct visual ecologies, with selection acting at the perceptual, processing and molecular level.

KEY WORDS: Allometric scaling, Apposition compound eye, Lepidoptera, Neuroecology, Optic lobe, Visual ecology

INTRODUCTION

The diversity of animal visual specialisations reflects their central role in key behaviours such as foraging, navigation, communication and predator avoidance (Cronin et al., 2014; Endler et al., 2005). As the maintenance of complex visual adaptations incurs significant energetic costs (Land and Nilsson, 2012; Laughlin et al., 1998; Moran et al., 2015; Niven et al., 2007; Niven and Laughlin, 2008), divergence in specialisation at any functional, physiological, anatomical or molecular level is likely the result of ecological selection pressures (e.g. Gonzalez-Bellido et al., 2011; Hofmann et al., 2009; Huber et al., 1997; Scales and Butler, 2016; Sugawara et al., 2005; Zhao et al., 2009). However, such specialisations are also limited by a number of trade-offs including evolutionary history, body size and other allometric and physiological constraints (Land, 1997; Land and Nilsson, 2012; Warrant and McIntyre, 1993). Understanding how an animal's visual ecology interacts with these constraints to shape variation in visual systems is a central question to sensory and neuroecology (Cronin et al., 2014; Lythgoe, 1979; Striedter, 2005).

Visual system diversity is greatest within the Arthropoda (Osorio et al., 1995; Stansbury and Moczek, 2013; Yilmaz et al., 2022). This diversity is perhaps best reflected by their colour vision, which is acquired via the tuning of visual pigments found within photoreceptor cells. These pigments consist of a retinal-based chromophore attached to an opsin protein, where the sequence of critical amino acid residues within the chromophore binding pocket of the opsin can shift the wavelength sensitivity, which varies between species with different visual ecologies (Fain et al., 2010; Feuda et al., 2016; Frentiu et al., 2007; Terakita, 2005). In apposition compound eyes, each facet typically projects light along a single rhabdom within an ommatidium, separated from adjacent ommatidia by light-absorbing pigments (Land, 1989). However, anatomical and physiological parameters such as total eye size, shape, lens diameter, acuity, sensitivity, number of ommatidia and pupillary response vary, even between closely related species (Bartholomée et al., 2023; Greiner, 2006; Greiner et al., 2004a; Land, 1989; Narendra et al., 2013; Scales and Butler, 2016; Somanathan et al., 2009; Warrant, 2001). For example, shifts to a nocturnal lifestyle have led to larger ommatidial facets and rhabdom diameters in the apposition eye morphology of the sweat bee, *Megalopta genalis*, compared with its close relatives (Greiner et al., 2004a; Warrant, 2017). Microhabitat partitioning within communities of Hawaiian damselflies and hemiboreal bumblebees has also resulted in rapid shifts in eye sensitivity at a much finer ecological scale (Bartholomée et al., 2023; Scales and Butler, 2016). Spatial variation in light abundance and spectral composition within habitats has also promoted compound eye regionalisation whereby different eye regions are fine-tuned to optimally receive ecologically relevant stimuli (e.g. Arikawa et al., 2009; Lehrer, 1998; Labhart and Meyer, 1999; Meyer and Labhart, 1992; Nilsson and Smolka, 2021; Nilsson et al., 2022; Stavenga, 1992; Stavenga et al., 2001; White et al., 2003; Zufall et al., 1989). For example, the dorsal rim area of many insects is specialised for polarisation vision, useful for orientation and navigation (Dacke et al., 2002; Mappes and Homberg, 2004; Reppert et al., 2004;

[1]School of Biological Sciences, University of Bristol, 24 Tyndall Avenue, Bristol BS8 1TQ, UK. [2]Bristol Palaeobiology Group, School of Earth Sciences, University of Bristol, 24 Tyndall Avenue, Bristol BS8 1TQ, UK. [3]Living Systems Institute, University of Exeter, Stocker Road, Exeter EX4 4QD, UK.

*Authors for correspondence (jw14637@bristol.ac.uk; s.montgomery@bristol.ac.uk)

J.B.W., 0000-0003-3689-1725; M.C., 0009-0008-1849-4463; D.P., 0009-0009-4379-9477; E.M.-S., 0000-0003-0139-2109; E.A.B., 0000-0001-7349-1494; M.J.H., 0000-0001-5135-8828; N.W.R., 0000-0002-4540-6683; S.H.M., 0000-0002-5474-5695

Received 18 July 2023; Accepted 31 October 2023

Journal of Experimental Biology (2023) 226, jeb246423. doi:10.1242/jeb.246423

Sauman et al., 2005; Stalleicken et al., 2006). The fine structure and function of the primary insect visual neuropils can also differ (Sinakevitch et al., 2003). Although the general structure of optic lobes is largely conserved, typically subdivided into four main synapse-dense regions (the lamina, medulla, lobula and lobula plate) (Fig. 1A; Strausfeld and Nässel, 1980), the way they have evolved to process different forms of visual information again reflects their visual environment and evolutionary history. For example, neural adaptations for spatial and temporal summation within the lamina are repeatedly associated with shifts towards nocturnal diel patterns (Greiner et al., 2004b; Warrant et al., 2004; Stöckl et al., 2016b, 2020).

Understanding how visual systems evolve in response to novel habitats requires comparative study systems of species with diverse and well-documented ecologies. Lepidopterans are one such group, occupying a wide range of light environments, relying heavily on the use of visual cues and signals for a variety of behavioural tasks, and exhibiting considerable levels of investment in specialised visual system physiology and anatomy (Bergman et al., 2021; Briscoe and Chittka, 2001; Couto et al., 2020; Nilsson et al., 1988; Stavenga and Arikawa, 2006; Stöckl et al., 2016a,b). Like other arthropods, lepidopteran species that occupy high-light-intensity environments tend to have larger optic lobe neuropils than species found in low-light habitats, or nocturnal conditions (Couto et al., 2020; Heinze and Reppert, 2012; Montgomery and Ott, 2015; Montgomery and Merrill, 2017; Wainwright and Montgomery, 2022). The opposite appears true for relative eye size, where nocturnal species have evolved larger facets and wider and longer rhabdoms to maximise light collection and absorption (Frederiksen and Warrant, 2008; Yack et al., 2007). However, in butterflies, there is also some evidence that visual systems vary across more subtle ecological differences, and readily adapt over short evolutionary scales. For example, a comparison of two *Boloria* butterfly species identified larger eyes and facets in the frontal eye region in *B. aquilonaris*, whose habitat is naturally fragmented relative to *B. eunomia*, suggesting that differences in eye morphology can evolve remarkably rapidly in response to ecological challenges (Turlure et al., 2016). Consistent patterns of neural divergence in response to ecological preference shifts have also been observed between parapatric *Heliconius* butterfly species, which also display eye structural variation, separated across continuous environmental gradients within tropical forests (Hebberecht et al., 2023; Montgomery and Merrill, 2017; Montgomery et al., 2021; Seymoure et al., 2015).

To better explore how visual systems evolve in response to subtle environmental changes we present here a detailed study of interspecific and intraspecific differences in both eye and brain structure, across representatives of a diverse 26-million-year-old tribe of Neotropical butterflies, the Ithomiini (Nymphalidae: Danainae) (Chazot et al., 2019). Historically, ithomiines have been primarily studied for their Müllerian mimicry rings (also referred to as mimicry complexes) where multiple species have evolved convergent wing colours, patterns and morphologies to amplify their aposematic signal to predators within sympatric communities (Bates, 1862; Beccaloni, 1997; Elias and Joron, 2015; Hill, 2021; Müller, 1879). Critically, for mimicry to be effective, co-mimics must signal to the same predators, whose distribution and abundance varies across forest habitats (Gompert et al., 2011; Willmott et al., 2017). As a result, data on forest structure suggest that mimicry rings are segregated across microhabitats, which likely expose closely related species from different mimicry rings to divergent visual environments (Beccaloni, 1997; Elias et al., 2008; Hill, 2010; Wainwright and Montgomery, 2022; Willmott et al., 2017). Typically, colourful ithomiine mimics are found in more open forest compared with cryptic, transparent-winged ithomiines, which reside in shaded inner forest (Elias et al., 2008; Pliske, 1975), and these habitat shifts have been linked to variation in investment in sensory neuropils (Montgomery and Ott, 2015; Wainwright and Montgomery, 2022). In addition, although ithomiines are generally not sexually dichromatic, evidence of dimorphism in olfactory and visual processing centres might hint at the possibility of additional sex-specific patterns of visual investment (Montgomery and Ott, 2015; Morris et al., 2021; Pliske, 1975; Wainwright and Montgomery, 2022).

Here, we focused on representatives of four subtribes within the ithomiine radiation: *Greta morgane* Geyer 1833 (subtribe: Godyridina), *Mechanitis polymnia* (Linnaeus 1758) (subtribe: Mechanitina), *Methona confusa* Butler 1873 (subtribe: Methonina) and *Tithorea harmonia* (Cramer 1777) (subtribe: Tithoreina) (Fig. 1B; Chazot et al., 2019; de Silva et al., 2010). *Mechanitis polymnia*, *M. confusa* and *T. harmonia* have converged on an open forest microhabitat, flying at high elevations (Elias et al., 2008), whereas the transparent *G. morgane* flies lower down in shaded forest understory (Fig. 1B; Elias and Joron, 2015; Willmott and Mallet, 2004). By combining results from selection analyses on opsin sequences from recent genomic data, ophthalmoscopy, micro-CT, immunohistochemistry and neural tracing, we describe and quantify variation for several aspects of the ithomiine visual system. Our data reveal multiple examples of anatomical, physiological and molecular variation within and between these four ithomiine species, highlighting potential adaptations for optimising visual perception and processing during microhabitat niche partitioning.

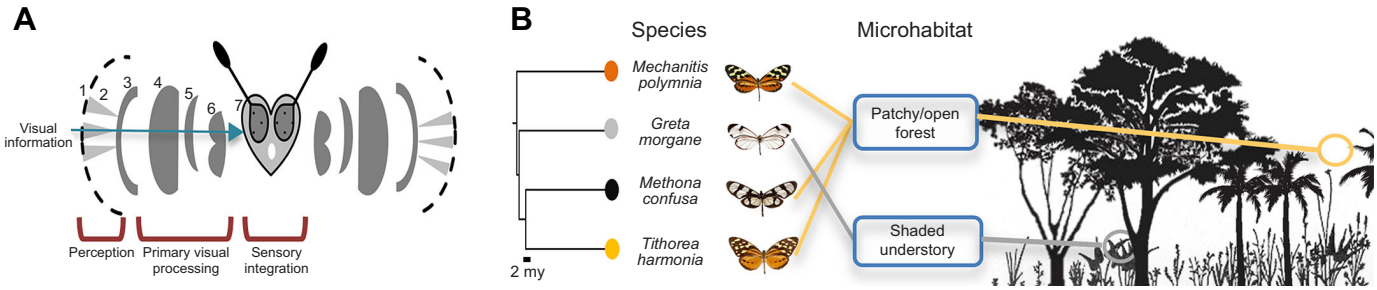

Fig. 1. An overview of butterfly visual systems and ecology of the four ithomiine study species. (A) Schematic diagram of a butterfly head representing the different levels of sensory organisation within the visual system: (1) facet; (2) ommatidia; (3) lamina; (4) medulla; (5) lobula plate; (6) lobula; and (7) central brain. (B) Microhabitat segregation in ithomiines coupled with a pruned molecular phylogeny calibrated by Chazot et al. (2019) to show the evolutionary relationships between the four study species.

Journal of Experimental Biology (2023) 226, jeb246423. doi:10.1242/jeb.246423

MATERIALS AND METHODS

Molecular analyses of visual opsins

Opsin gene alignment and data mining

Opsin sequences for *Danaus plexippus* (Nymphalidae: Danainae), the most closely related species to the Ithomiini for which all three visual opsins (ultraviolet, blue and long-wavelength) are publicly available on GenBank, were used as query sequences. These sequences were utilised for finding homologous opsins within recently assembled genomes of each of four ithomiine species (F. C. Cicconardi, B. J. Morris and S. H. Montgomery, unpublished) using Exonerate v2.2.0 with '-model protein2genome' and '-percent 50' options (Slater and Birney, 2005; Zhan and Reppert, 2012). To increase the power of our comparative analyses, we used GenBank deposited ultraviolet (UV), blue (B) and long-wavelength (LW) opsin sequences from 13 additional nymphalid butterfly species with well-established ecologies (all sequences used in our analyses, including accession IDs, can be found in Table S1).

To confirm functional opsin number for each ithomiine species, the transmembrane structure of each opsin sequence was predicted using Phobius, implemented through Protter (Kall et al., 2007; Omasits et al., 2014), a webserver-based tool for making protein structural predictions. Any opsin sequences predicted to have six or seven transmembrane domains were considered putative functional opsins. Rh7 opsins were also surveyed; however, this gene family was not included in downstream analyses owing to a poor abundance of other available nymphalid Rh7 sequences, as previously noted by Sondhi et al. (2021). The 3D protein structure for the *G. morgane* and *T. harmonia* UV opsins were also modelled using a homology-based approach in Swiss-Model (Waterhouse et al., 2018). The jumping spider Rhodopsin-1 (9i9k.1.A) was used as a template because this had the highest identity score and coverage (*G. morgane*: GMQE=0.67, identity=37.39; *T. harmonia*: GMQE=0.68, identity=38.34).

Gene tree estimation

Gene sequences for each opsin family (UV, B, LW) were aligned separately using MACSE v2 (Ranwez et al., 2018), a tool that accounts for underlying codon structure when aligning protein-coding nucleotide sequences. Aligned sequences were manually cleaned and trimmed in SeaView v5 (Gouy et al., 2021) to ensure the alignment contained no stop or incomplete codons. The final alignments all contained approximately 1100 nucleotide bases with 370 amino acids, which falls within the range of previously characterised lepidopteran opsin sequences (White et al., 2003; Zhan and Reppert, 2012). IQ-TREE (multi-core v1.6.12) was then used to build a maximum likelihood (ML) nucleotide gene tree for each opsin from these alignments (iqtree -s alignment_name.fasta -st DNA -bb 10,000 -nt AUTO -alrt 1000) using ModelFinder and ultrafast bootstrap (Fig. 2A; Hoang et al., 2018; Kalyaanamoorthy et al., 2017; Trifinopoulos et al., 2016).

Selection analyses

We tested whether an ecological shift from open to shaded forest was associated with relaxed or intensifying selection on the visual opsins of *G. morgane* by applying RELAX implemented in HyPhy, accessed via the Datamonkey webserver (Kosakovsky Pond et al., 2020; Wertheim et al., 2015). When given prespecified test (T) and reference (R) branches from the gene tree, RELAX estimates the rate of nonsynonymous to synonymous nucleotide base substitutions (d_N/d_S, or ω) among three rate categories using a BS-REL (branch site random effects likelihood) model (Kosakovsky Pond et al., 2011) before raising these values to the parameter k (ω^k) in T, which estimates the strength of selection at T relative to R. When k=1, as is the case in the null model, the ω distributions of T and R are the same. If k<1, T is under relaxed selection relative to R, whereas if k>1, T is under intensified selection relative to R (Wertheim et al., 2015). Null and alternative models are then compared with likelihood ratio tests using a χ^2 distribution. In our analyses, the *G. morgane* branch tip was specified as T for each opsin class with all other branches being assigned to R, with the exception of the UV opsin analysis, where duplicated opsins were included, with these portions of the tree being left as unspecified branches. Additional tests were performed to compare patterns of selection following gene duplications, where the branch stemming from the duplicated node was specified as T and all other branches assigned as R.

Animals for physiology and anatomy

Butterflies used in physiological and anatomical comparisons were purchased as pupae or as live adults from The Entomologist Ltd (*M. polymnia*, *M. confusa* and *T. harmonia*) and Tropical Butterflies UK (Edu-Sci Ltd) (*G. morgane*), respectively. Individuals were reared in 2.2×1.8×1.8 m cages kept at 28–35°C and 80% relative humidity at the University of Bristol's Old Park Hill Greenhouse facility and were regularly fed 30% sucrose solution. Adults were marked and sexed immediately post-eclosion and matured for a minimum of 3 days before being sampled.

Eye physiology comparisons

Ophthalmoscopy

Interspecific and intraspecific variation in eye physiology were explored using a custom-built ophthalmoscope (Fig. S1), based on the system described by Brodrick et al. (2020). It consisted of a UI-3590CP-C-HQ-R2 camera with a CMOS colour sensor (Imaging Development Systems, Germany), 10×0.25 NA objective lens (Plan N, Olympus, Tokyo, Japan), beam-splitter (Thorlabs, Newton, MA, USA) and a portable fibre-coupled broadband (470–850 nm) LED (MBB1F1 Thorlabs, Munich, Germany), which was projected along an optical fibre, providing co-axial illumination of the eye. The camera was connected to a computer with a uEye Cockpit program (part of the IDS Software Suite 4.95) installed for capturing and recording images and videos.

Twelve live individuals of each of the four species were used in the investigation, with approximately equal numbers of males and females (Table S2). Intact butterflies were mounted in slotted plastic tubes and further immobilised using plasticine before being suspended at the centre of rotation of a Newport M-MGM80MS 90 deg rotation goniometric cradle by attaching the plastic tube to the arm of a micromanipulator (Fig. S1). Butterflies were then oriented to set the eye's direction of view. The ophthalmoscope was adjusted to focus on a region of the cornea where the optical axes of several ommatidia are directly facing the objective lens, thus viewing the individual's pseudopupil. After dark adapting for as briefly as 10 s, the LED can be switched on to reveal the eyeshine (or luminous pseudopupil) created by unabsorbed light reflecting off a mirror-like tracheolar tapetum at the proximal end of each rhabdom (Franceschini and Kirschfeld, 1971; Stavenga, 1979, 2002). Unabsorbed reflected light leaves the eyes, referred to as eyeshine, the colour and heterogeneity of which varies hugely between butterfly species (Belušič et al., 2021; Briscoe and Bernard, 2005; Stavenga et al., 2001). As expected, the intensity of this eyeshine diminished within seconds of illumination owing to the intracellular migration of pigment granules, which move from the soma towards the rhabdomeres, preventing light from reaching the tapetum (Qiu et al., 2002; Stavenga et al., 1977). This is referred

Journal of Experimental Biology (2023) 226, jeb246423. doi:10.1242/jeb.246423

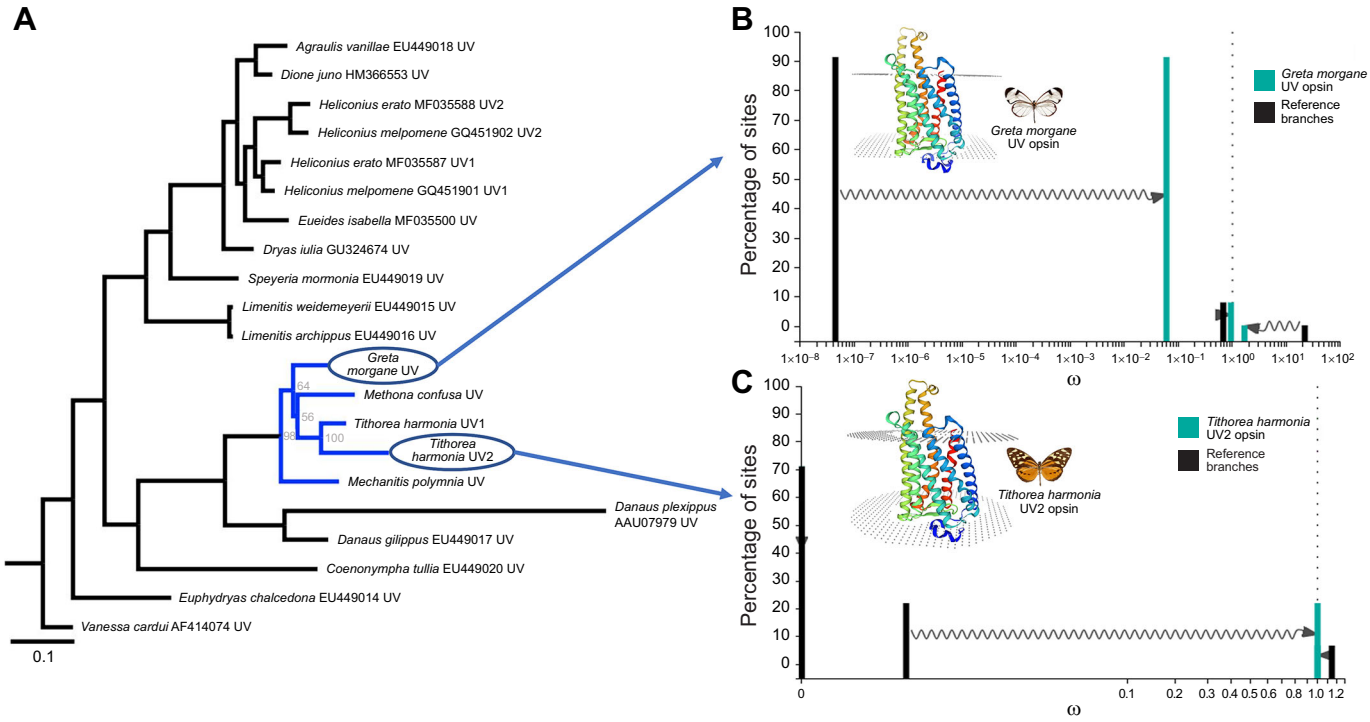

Fig. 2. Signatures of relaxed selection in ithomiine UV visual opsins. (A) Maximum likelihood nucleotide gene tree created using IQ-TREE which includes all UV opsin sequences used in our analyses. Ithomiine branches are highlighted in blue, for which the ultrafast bootstrap values calculated from 10,000 replicates are displayed at the nodes. (B) Comparison of ω distributions between the *Greta morgane* UV test branch (turquoise) and all other reference branches under the alternative model of relaxed selection. The branch tips leading to the duplicated UV2 opsins of *Heliconius melpomene* and *Tithorea harmonia* were left as unspecified in the RELAX analysis. (C) Comparison of ω distributions from the newly discovered UV2 opsin of *T. harmonia* under the alternative relaxed selection model when compared to all other reference branches. Branches leading to the *G. morgane* UV and *H. melpomene* UV2 opsins were left unspecified. In both B and C, sites under purifying (ω>1) or positive (ω<1) selection in the reference move towards neutrality in the test branch (ω=1). Arrows indicate that when comparing sites in the prespecified test and reference branches, all three ω distributions used in the BS-REL model (corresponding to sites under strong purifying, weakly purifying and positive selection) shift closer towards neutrality in the test branches. Superimposed on both B and C is a 3D protein model of the *G. morgane* UV and *T. harmonia* UV opsin, respectively, created using Swiss-Model (Waterhouse et al., 2018) with the jumping spider rhodopsin-1 as the template. Prediction of alpha helices are shown in different colours, and areas between the top and bottom dotted layers indicate transmembrane predictions.

to hereafter as the pupillary response. We used the duration of the pupillary response to assay how rapidly eyes physiologically respond to sudden changes in their light environment.

Video recordings of the eyeshine were taken in the dorsal, frontal and ventral eye regions (achieved by rotation of the goniometric cradle) after 10 min of dark adaptation under standard laboratory conditions (21°C). When video recordings were made in the frontal eye region, individuals were also dark adapted for 0.5, 1, 5 and 20 min, in a randomised order, to confirm whether any interspecific patterns are still observed for different lengths of dark adaptation. We also recorded whether the rate of habituation to a flashing light stimulus differed between species by switching the LED light source on and off at 10 s intervals for a period of 5 min. Here, our intention was to simulate changes in light conditions as individuals transition between microhabitats. Videos were imported into FIJI/ImageJ (Schindelin et al., 2012), where response time was visualised and estimated using the View5D plugin (Fig. 3A). Reflecting facets were counted and categorised as being red or yellow, where red-reflecting ommatidia indicate the presence of LW-shifted photoreceptors. Using this, the ratio of yellow:red ommatidia was also calculated for the frontal region of each individual.

Once eye physiological data had been collected, half of the individuals from the eyeshine study were sampled for micro-computed tomography (micro-CT; see 'Micro-computed tomography'). The second half of individuals from the eyeshine experiment were sampled for immunohistochemistry (see 'Neuroanatomical comparisons').

Statistical analysis

All statistical analyses were performed in R (https://www.r-project.org/). Following Shapiro–Wilk tests for normality and Bartlett's test for homogeneity of variances, linear models were constructed, testing the effect of species, sex and their interaction on response time in the frontal region. Subsequent *post hoc* comparisons were performed using the Tukey HSD function. Similar analyses were also performed to test for species and sex differences in response time in the habituation experiment. The ratios of yellow:red reflecting frontal ommatidia did not follow a normal distribution, so the non-parametric Kruskal–Wallis test was performed instead. Intraindividual differences in the number of reflecting ommatidia and response time between eye regions were analysed by building linear models with the mean fitted as a fixed effect, the null hypothesis being that the mean difference between eye regions is zero. For the analysis of response time, species, sex and their interaction were included as additional independent variables.

Micro-computed tomography

Image acquisition

Heads were severed and placed directly into a chilled fixative (4% paraformaldehyde, 2% glutaraldehyde, 2% glucose) in 0.1 mol l^{-1}

Journal of Experimental Biology (2023) 226, jeb246423. doi:10.1242/jeb.246423

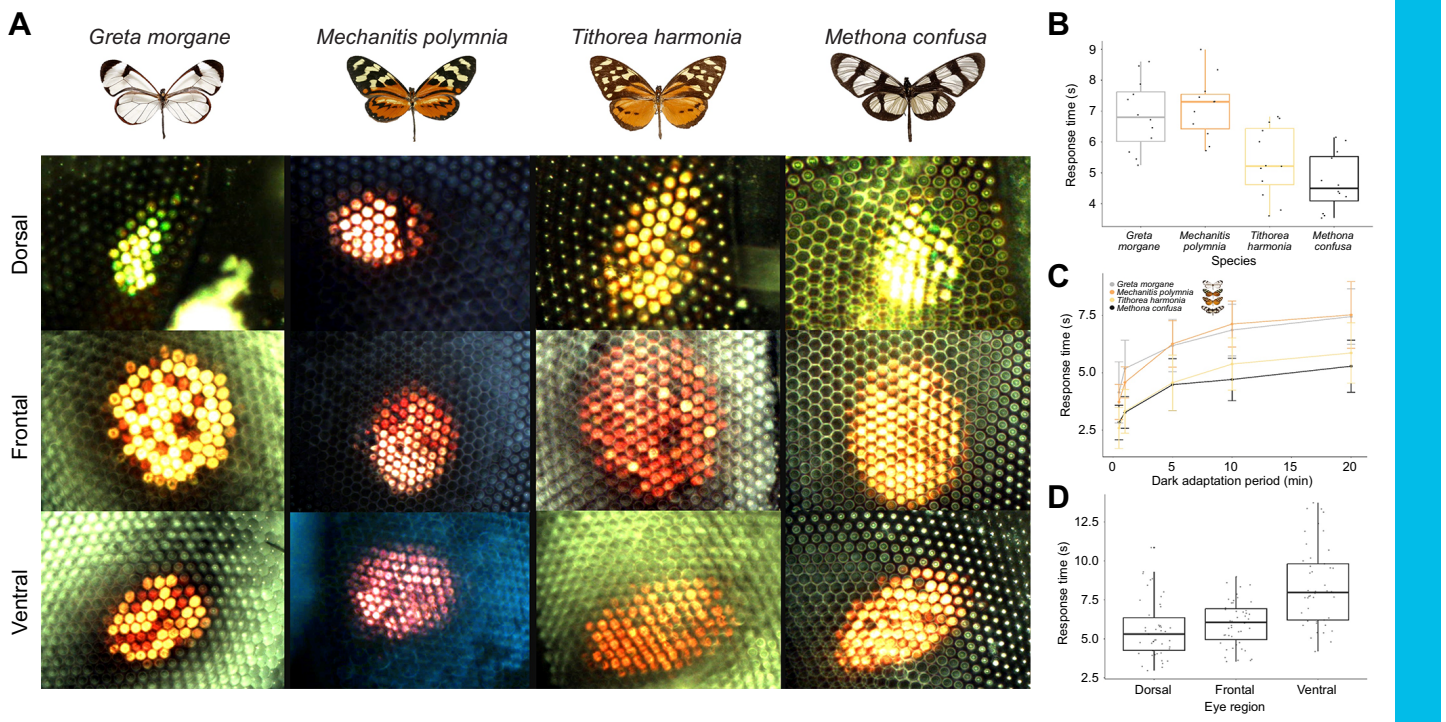

Fig. 3. Ithomiine eyeshine variation (*n*=48, 54.17% female). (A) Ophthalmoscope images of the dorsal, frontal and ventral luminous pseudopupil within a single individual of all four study species after 10 min of dark adaptation. (B) Interspecific differences in frontal pupillary response time. (C) Frontal pupillary response time after different lengths of dark adaptation. Points show means for each species (*n*=12 per species, 50–58% female) with error bars representing standard deviation. (D) Intraindividual differences in pupillary response time for the dorsal, frontal and ventral eye regions. For all boxplots, medians (thick horizontal bars), interquartile ranges (boxes), values within 1.5 interquartile ranges of the box edges (whiskers) and possible outliers (data points outside the whiskers) are plotted.

sodium phosphate buffer solution (pH 7.4) for 24 h under agitation. Heads were dehydrated in a graded ethanol series (10%, 30%, 50%, 70%, 90%, 95%, 10 min each), before being stained with 1% iodine dissolved in 100% ethanol for 3 days under agitation to enhance X-ray absorption contrast (Smith et al., 2016; Swart et al., 2016). Samples were subsequently washed in 100% ethanol three times, each for 30 min, and stored in ethanol at 4°C until ready for use. The body mass (g) of each individual was also recorded.

Tomographic images of the samples were taken at the University of Bristol's X-ray tomography (XTM) facility using a Nikon XTH225ST scanner with a 180 kV transmission target. Heads were typically imaged using ×0.33 total magnification and a ∼2.2 µm effective pixel size (see Table S5 for full scanning parameters). In total, 23 heads were scanned (*n*=6 per species with the exception of *T. harmonia*, where one individual experienced bacterial growth and was thus removed from any subsequent analyses; see Table S3). Scan acquisition and reconstruction was achieved using Nikon CT Pro and the resulting TIF files were exported using VG Studio MAX (Fig. 4A). The resolution of the micro-CT scans allowed identification of the corneal lens of each ommatidium, as well as the area where the crystalline cones and light-sensitive rhabdoms are located (Fig. 4B–D).

Eye volumetric reconstructions

The resulting TIF stacks were compressed from 32 bit to 8 bit and cropped in FIJI/ImageJ (Schindelin et al., 2012). They were then loaded into Amira 3D 2021.2 (ThermoFisher Scientific, FEI Visualization Sciences Group). Label files were created for each individual using the labelfield module, and segmentation was performed by manually delineating the boundaries of the eye based on intensity contrasts (Fig. 4C,D). Features were labelled every 5–10 slices before being interpolated so all intervening slices could be assigned to the structure of interest. Reconstructions were edited and smoothed before total volumes were extracted using the measure statistics module. The volume of each bilaterally paired structure was then multiplied by two and $\log_{10}$ transformed before any analyses.

Eye anatomical measurements

Further anatomical measurements were made with the 3D Measurement tool in Amira to manually estimate ommatidial length (L, µm), interommatidial angle ($\Delta\Phi$, deg) and facet diameter (D, µm) (Fig. 4D,E). Five to 10 measurements of L, $\Delta\Phi$ and D were taken in each eye region with a mean calculated per region per individual. Eye regions were defined in the x–y dimension with the upper, middle and lower thirds of the eye comprising the dorsal, frontal and ventral eye regions, respectively. In practice, no measurements were taken in ambiguous regions and the distribution of dorsal and ventral measurements are skewed towards the extreme ends of those boundaries as a result. To minimise measurement error when estimating D, the width of five adjacent facets were measured before dividing by five. We also measured interocular distance (IOD, µm), defined as the minimum horizontal gap between the two compound eyes when viewed in the x–y dimension, to provide an allometric control in our statistical analyses. As was the case for the volumetric reconstructions, all eye anatomical data were $\log_{10}$ transformed before any analyses.

Statistical analysis

To test for allometric scaling differences, linear models were constructed where each measurement of interest was scaled against IOD, with species, sex and their interaction included as additional independent variables. If significant species or sex effects were

Journal of Experimental Biology (2023) 226, jeb246423. doi:10.1242/jeb.246423

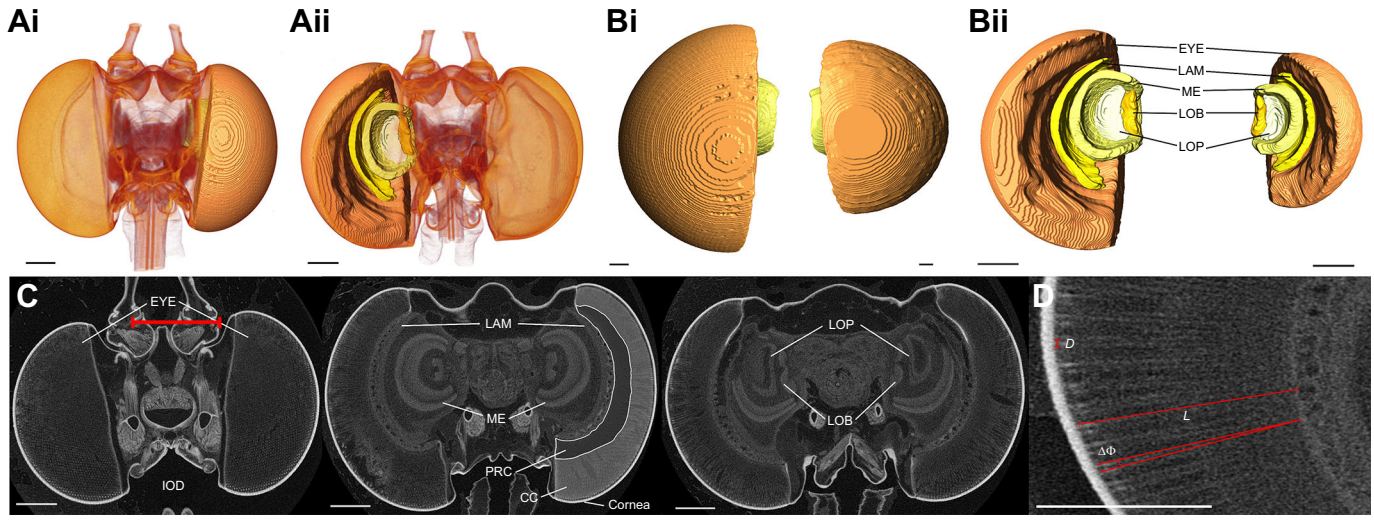

Fig. 4. An eye and brain anatomical overview for the ithomiine species using micro-CT data (*n*=23, 52.17% female). (A) Volume rendered whole-head images from micro-CT scans of *Methona confusa* from the anterior (i) and posterior (ii) with surface reconstructions of the eye and the four primary optic neuropils of interest superimposed on the right. (B) Anterior (i) and posterior (ii) surface reconstructions of the eye (EYE), lamina (LAM), medulla (ME), lobula (LOB) and lobula plate (LOP) of *M. confusa* (left) and *Greta morgane* (right), shown to scale. (C) Iodine-stained micro-CT X-ray tomography frontal sections of *M. confusa* taken at progressively posterior positions through the head, moving from left to right. Additional labels are the cornea, the areas containing crystalline cones (CC) and photoreceptor cells (PRC) and an exemplification of our measure of interocular distance (IOD). (D) Further exemplifications of our measures of facet diameter (*D*), ommatidial length (*L*) and interommatidial angle (ΔΦ) from sections of the same *M. confusa* individual. Scale bars: 200 µm.

detected, *post hoc* pairwise scaling comparisons were made by building standardised major axis regressions using the sma function in the smatr package (Warton et al., 2012). This function tests for group-level deviation from a common scaling relationship between two traits, modelled as log y=βlog$x$+α. We first tested for conservation in the allometric slope (β), deviation from which would suggest an effect of species or sex in how each dependent variable interacts with IOD. If equal slopes were found, the presence of a 'grade shift' (change in α) along the y-axis was examined, a common indicator of adaptive sensory divergence (Farnworth and Montgomery, 2022; Kruska, 2005; Montgomery et al., 2016a,b; Sylvester et al., 2011). Facet diameter (*D*) did not scale with IOD (or central brain or body size), suggesting that any differences between species occur independently of allometric scaling. Therefore, we tested for differences using the absolute, untransformed *D* values. Intraindividual differences in eye structure between dorsal, frontal and ventral eye regions were analysed by applying the same statistical methods used for the eyeshine data, described above.

Neuroanatomical comparisons

Immunohistochemistry

Brain dissections were conducted under HEPES-buffered saline (HBS; 150 mmol l^{-1} NaCl; 5 mmol l^{-1} $CaCl_2$, 25 mmol l^{-1} sucrose; 10 mmol l^{-1} HEPES; pH 7.4) with brains subsequently fixed in zinc formaldehyde solution [ZnFA: 0.25% (18.4 mmol l^{-1}) $ZnCl_2$, 0.788% (135 mmol l^{-1}) NaCl, 1.2% (35 mmol l^{-1}) sucrose, 1% formaldehyde] for 16–20 h under agitation, as in Ott (2008). Brains were washed three times in HBS and placed in Dent's solution (80% methanol/20% DMSO) for ∼2 h under agitation. They were then placed in 100% methanol for 1 h at room temperature before being transferred to fresh methanol and stored at −20°C until later use.

Rehydrated brains were embedded in agarose gel (5% UltraPure agarose power in deionised water) and sectioned using a vibrating blade microtome with an 80 µm interval (Leica VT1200, Wetzlar, Germany). Sections were then washed six times in PBS-TX (0.5% Triton X-100 detergent in phosphate-buffered saline), 5 min each, before being incubated in 5% normal goat serum (NGS) dissolved in PBS-TX (NGS-PBS-TX; NGS; New England BioLabs, Hitchin, Hertfordshire, UK) for a minimum of 1 h at room temperature. Samples were then stained with anti-allatostatin (Antibody 5F10; Developmental Studies Hybridoma Bank, University of Iowa, Iowa City, IA, USA, RRID: AB_528076) at a 1:100 dilution in fresh NGS-PBS-TX and incubated for 24 h at room temperature under agitation. Allatostatin is a neuropeptide expressed in distinct cell types within the optic lobes of insects and crustaceans (Kreissl et al., 2010; Lin et al., 2021; Sivasubramanian and Sood, 2003) and provides additional anatomical detail of these brain regions. Slices then underwent 6×30 min PBS-TX washes before introducing the secondary Cy2-conjugated anti-mouse antibody (Jackson ImmunoResearch cat. no. 115-225-146, RRID: AB_2307343, West Grove, PA, USA) at a 1:100 dilution in fresh NGS-PBS-TX. Samples were left in the dark at room temperature for a further 24 h before undergoing 6×30 min PBS-TX washes, and were then added to 60% glycerol in PBS and left overnight. Slices were then transferred to 80% glycerol in PBS before mounting on glass slides with excess 80% glycerol solution under a cover slip, sealed with nail varnish.

Dextran tracing and wholemount immunohistochemistry

In a separate sample of individuals, we performed *in vivo* dextran injections to explore neural connections between the optic lobe and structures within the central brain. Live butterflies were kept in custom-made slotted plastic holders and immobilised using dental wax. A small window was made in or just behind the compound eye, so part of the optic lobe was exposed. For some individuals, a window was made above the dorsal central brain instead to allow access to the mushroom bodies. A few crystals of dextran tetramethylrhodamine (Invitrogen™ D1868, Fisher Scientific, Leicestershire, UK) were dissolved in bovine serum albumin (BSA, Merck Life Science UK Ltd, Gillingham, Dorset, UK) and

placed on the tip of a horizontally pulled glass electrode (tip diameter ∼200 µm). Dextran was manually inserted into either both optic lobes or both mushroom bodies calyces under red-filtered light using a dissection microscope. Any remaining dextran on the brain surface was rinsed off with Ringer's solution (150 mmol l^{-1} NaCl, 3 mmol l^{-1} $CaCl_2$, 3 mmol l^{-1} KCl, 2 mmol l^{-1} $MgCl_2$, 10 mmol l^{-1} HEPES, 5 mmol l^{-1} glucose, 20 mmol l^{-1} NaOH, pH 6.9). The intact butterfly head was then left submerged in Ringer's solution for a minimum of 4 h at room temperature to allow the dextran to be transported to the terminal projection sites of affected neurons. The brain was then dissected and stored using the protocols described above.

To reveal neuropil structure, injected brains were stained as wholemounts using indirect immunolabelling against synapsin (Antibody 3C11; Developmental Studies Hybridoma Bank, RRID: AB_2315424), a conserved insect protein expressed at presynaptic regions (Brandt et al., 2005; Heinze and Reppert, 2011; Klagges et al., 1996; Montgomery and Ott, 2015). Brain samples were rehydrated in a decreasing methanol-Tris buffer dilution series (90%, 70%, 50%, 30%, 0%, pH 7.4) for 10 min each. Samples were incubated in NGS (New England BioLabs, Hitchin, Hertfordshire, UK) diluted in 0.1 mol l^{-1} PBS (pH 7.4) and 1% DMSO for 2 h at room temperature, before the primary antibody was added at a 1:30 dilution with fresh NGS-PBSd and left at 4°C for 3.5 days under agitation. Non-bound primary antibody was removed after three 2 h PBSd washes before introducing the secondary Cy2-conjugated anti-mouse antibody at a 1:100 dilution in NGS-PBSd and left in the dark at 4°C for a further 2.5 days under agitation. Samples were then washed in glycerol diluted in 0.1 mol l^{-1} Tris buffer (1% DMSO) in an increasing dilution series (1%, 2%, 4%, for 2 h each, 8%, 15%, 30%, 50%, 60%, 70%, 80%, for 1 h each) under agitation. Samples were dehydrated and washed in 100% ethanol three times, for 30 min each, before clarification by underlaying the ethanol with methyl salicylate.

Confocal microscopy

All immunostained brains were imaged on a confocal laser-scanning microscope (Leica SP5-AOBS/SP5-II, Leica Microsystems, Mannheim, Germany) at the University of Bristol's Wolfson Bioimaging Facility, using either a 10×0.4 NA or 20×0.7 NA objective lens (Leica Material nos 506285, 506513, Leica Microsystems). Single-capture images of wholemounts and sections were achieved with a 488 nm argon laser (20% intensity), and an *x*–*y* resolution of 512×512 pixels. For dextran-traced individuals, an additional 580 nm argon laser channel (20% intensity) was included and scanned sequentially with the 488 nm laser to visualise the passage of dextran dye against the synapsin-stained background.

Volumetric comparisons

Volumetric reconstructions of the four primary optic neuropils (lamina, medulla, lobula plate and lobula) were obtained from the micro-CT scans using the same methods described above (see Fig. 7A). Paired neuropils were doubled and $\log_{10}$ transformed and analysed using the same statistical methods as the eye volumetric data. To test for associations between physically and functionally linked visual structures, a covariance matrix for the volumetric data was built by running multiple linear regressions with each structure of interest as a dependent variable and species as a random effect. We then tested for species and sex differences after accounting for these covariances by including species and sex as additional independent variables in these regressions.

RESULTS

Evidence of duplication and habitat-related relaxation of selection in UV opsins

We recovered single copies of UV, B and LW-sensitive opsins in the genomes of all four ithomiine species, except for *T. harmonia*, where two putative full-length UV opsin sequences containing no stop codons were identified. Our selection analyses revealed the UV opsin of the shade-dwelling *G. morgane* to show a significantly lower rate of nonsynonymous to synonymous nucleotide base substitutions relative to all assigned 'open habitat' reference branches (Fig. 2B; UV opsin, relaxation parameter, k=0.17, χ^2 test P=0.016) when contrasted against the null model, where all test and reference branches are assumed to be under the same selection pressures, indicating relaxed selection (see Materials and Methods). This null model was found to hold true when the same analyses were repeated on the B and LW opsin sequences (B opsin, k=22.21, P=0.314; LW opsin, k=0.290, P=0.174). The duplicated UV opsin of *T. harmonia* also showed signatures of significant relaxed selection (Fig. 2C; k=0.000, P<0.001), potentially indicative of ongoing pseudogenization. Therefore, our results may suggest shifts in selective regime operating at the molecular level, mediated by both habitat preference and gene duplication, which together might drive further variation in how visual systems respond to light.

The response to light varies across the eye and between species

We found significant variation in the retinal mosaic (Fig. 3) between species in the frontal region (yellow:red reflecting frontal ommatidia, χ^2=16.678, d.f.=3, P=0.001). *Greta morgane*, *M. polymnia* and *T. harmonia* all had distinguishable red- and yellow-reflecting facets, where *T. harmonia* contained a greater proportion of red-reflecting ommatidia. *Methona confusa* displayed more homogeneous orange eyeshine patterns (which were classified as yellow in the above analysis) (Fig. 3A, Table S4A). Therefore, three out of four species showed evidence of a red-sensitive spectral channel. The number of shining ommatidia within each pseudopupil was greatest in the frontal region (dorso-frontal, t=12.830, d.f.=37, P<0.001; fronto-ventral, t=3.540, d.f.=37, P=0.003; Table S4D), suggesting that this is where spatial resolution is at its highest. The dorsal region contained the fewest shining facets.

When testing for differences in frontal pupillary response time, we found evidence of significant interspecific variation in response time (F=15.870, d.f.=3, P<0.001) with no sex or interaction effects between species or sex (Fig. 3B, see Table S4B). *Post hoc* analysis revealed that overall, *G. morgane* and *M. polymnia* had longer response times regardless of the length of dark adaptation (Fig. 3C, Table S4B). Response time decreased after 5 min of exposure to a flashing light stimulus (t=2.354, d.f.=46, P=0.011), but no differences in this habituation time were found between species, sex or their interaction (see Table S4C). Finally, the pupillary response of ventral ommatidia was significantly longer than those in the dorsal (t=5.460, d.f.=46, P<0.001) and frontal (t=5.121, d.f.=46, P<0.001) eye regions, with no significant species, sex or interaction effects (Fig. 3D). Significant species differences were only found when testing for dorso-frontal variation (F=11.627, d.f.=3, P<0.001) (Table S4E).

Eye structure varies between species, sexes and eye regions

Micro-CT scans revealed quantifiable differences in overall eye size and structure between species (Fig. 4A,B). Each ommatidium within the apposition compound eye consists of a corneal lens and a

Journal of Experimental Biology (2023) 226, jeb246423. doi:10.1242/jeb.246423

deep crystalline cone that directs light through to the light-sensitive rhabdom where the photoreceptor cells are located (Figs 1A and 4C, D). Relative eye volume varied significantly between species (F=6.232, d.f.=3, P=0.007) when scaled against IOD. Allometric analysis also revealed that these differences were a result of grade shifts along the y-axis (Wald $\chi^{2=}$8.483, d.f.=3, P=0.037, (Fig. 5A), with *G. morgane* investing more in eye volume than the similarly sized *M. polymnia* (Table S6), for example. Significant grade shifts were also observed between *M. confusa* and *T. harmonia*, with the latter sharing the same scaling relationship as its co-mimic, *M. polymnia* (Fig. 5A).

Frontal and ventral ommatidial length (L) also varied between species (frontal region, F=4.292, d.f.=3, P=0.024; ventral region, F=4.048, d.f.=3, P=0.029) with significant, non-allometric interspecific grade shifts found for both eye regions (frontal, Wald χ^2=23.08, d.f.=3, P<0.001; ventral, Wald χ^2=15.23, d.f.=3, P=0.002; Fig. 5B). For frontal ommatidia, pairwise comparisons revealed *G. morgane* to have relatively longer ommatidia than tiger-stripe co-mimics *M. polymnia* and *T. harmonia*, which showed a conserved scaling relationship (Table S6C). Interommatidial angle ($\Delta\Phi$) did not show any significant species differences when scaled against IOD, suggesting that variation in this trait is largely determined by variation in head size (Table S6A). Testing for differences in the absolute, untransformed values for facet diameter (D) revealed significant interspecific variation for the frontal and ventral eye regions (frontal, F=8.429, d.f.=3, P=0.006; ventral, F=6.373, d.f.=3, P=0.015; Fig. 5C). *Post hoc* comparisons of these models showed that the majority of significant pairwise contrasts were with *M. polymnia*, which had consistently the narrowest facets (Fig. 5C, Table S6B).

Across the four species, evidence of sexual dimorphism was observed for relative eye volume (F=17.358, d.f.=1, P=0.001), with males displaying an increased investment in eye size (Wald χ^2=12.37, d.f.=1, P<0.001, (Fig. 5D). However, our sample sizes were insufficient to detect whether these differences in eye volume were explained by any other measured eye anatomical traits (Fig. 5E,F). We found no interactions between sex and species for any anatomical variables.

Finally, comparing intraindividual variation in eye anatomy, we found significant variation between the dorsal, frontal and ventral eye regions from the micro-CT scans (Fig. 5G–I). After multiple test correction, no species, sex or interaction effects were found, with the exception of D (where dorso-frontal differences between species were observed for females but not males, see Table S6E for details), suggesting these differences are mostly consistent across all individuals and species. Dorsal ommatidia were shorter and narrower than frontal and ventral ommatidia (Table S6E), and the $\Delta\Phi$ of dorsal ommatidia was significantly greater than the other two eye regions (dorso-frontal, t=8.949, d.f.=22, P<0.001; dorso-ventral, t=5.342, d.f.=22, P<0.001).

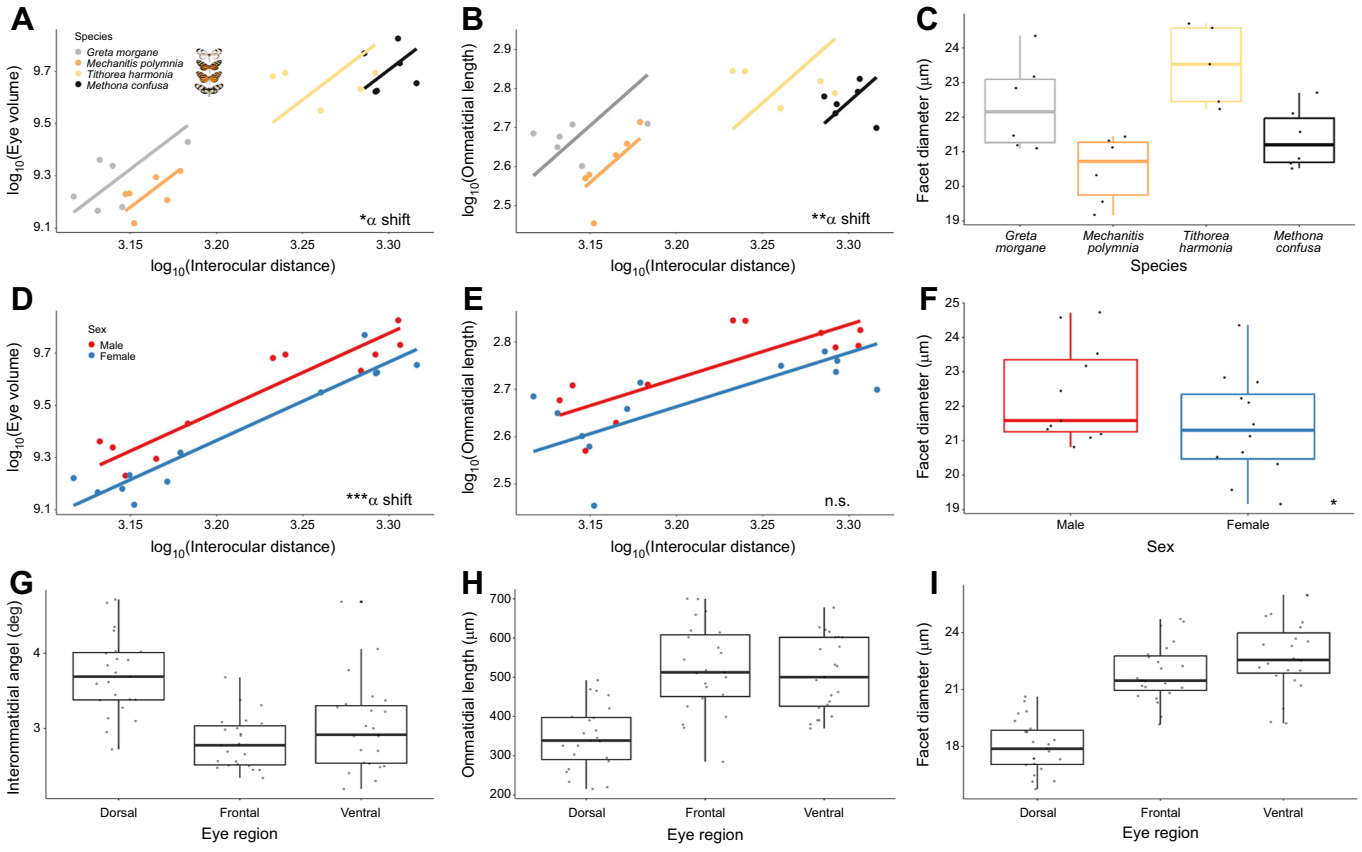

Fig. 5. Eye anatomical variation in four ithomiine species from micro-CT measurements (n=23, 52.17% female). (A–C) Interspecific differences in total eye volume (EYE, A), ommatidial length (L, B) and facet diameter (D, C). (D–F) Intersexual variation in EYE (D), L (E) and D (F). For EYE and L, log-transformed values are scaled against interocular distance (IOD), where an 'α shift' denotes a grade shift in the relationship between these two variables from our SMATR analysis. (G–I) Intraindividual differences in interommatidial angle ($\Delta\Phi$, G), L (H) and D (I) between the dorsal, frontal and ventral eye regions. For all boxplots, medians (thick horizontal bars), interquartile ranges (boxes), values within 1.5 interquartile ranges of the box edges (whiskers) and possible outliers (data points outside the whiskers) are plotted. n.s. P>0.05, *P<0.05, **P<0.01, ***P<0.001.

Journal of Experimental Biology (2023) 226, jeb246423. doi:10.1242/jeb.246423

Gross composition of optic lobe neuropils is generally conserved across species but there is evidence of sexual dimorphism in the presence of the ventral lobula

Staining against allatostatin revealed the retinotopic organisation of the optic lobe, particularly within the lamina and medulla, where the respective cartridge and column modules are clearly visible (Fig. 6A). Distinct layers of neuronal organisation are present in the medulla, consisting of two major outer and inner divisions, separated by the serpentine layer, as seen in other ithomiines (Montgomery and Ott, 2015). Within each division are several further striations, where a maximum of seven medulla layers were clearly observed in the scans of all four species (Fig. 7A). The lobula plate and the lobula have two and three layers, respectively, as observed in other Lepidoptera (e.g. Hamanaka et al., 2012). Two smaller neuropils, the accessory medulla, found against the anteromedial edge of the medulla, and the ventral lobula, an ovoid ventromedial structure that forms a close physical association with the lobula, were more clearly visibile in whole-mount anti-synapsin stains. Our samples suggest that the ventral lobula, which is smaller in ithomiines than in other butterflies where it has been identified (Wainwright and Montgomery, 2022), is sexually dimorphic in *G. morgane* and *M. polymnia*, being totally absent in all males of these species (Fig. 6B). In *Papilio xuthus* and Heliconiini butterflies, the ventral lobula appears to act as a relay centre between the optic lobe and the mushroom body calyx (Couto et al., 2023; Kinoshita et al., 2015). However, our dextran injections provided no evidence that the ventral lobula serves this purpose in ithomiines. The ventral lobula appears to receive inputs via the lobula, without innervation in the lobula plate (Fig. 6C), reminiscent of *Drosophila* medulla projection (Tm) neurons, which receive direct synaptic inputs from photoreceptors and relay this directly to the lobula (Borst, 2009; Lin et al., 2015). Our dextran injections suggested the ventral lobula then projects to the bulb in the central brain, a structure that forms part of the anterior visual pathway in *Drosophila* (Hardcastle et al., 2021; Lovick et al., 2017; Omoto et al., 2017). Dextran staining in the anterior optic tubercle, the main optic neuropil in the central brain, was also found for some individuals, but the precise neuronal inputs to this region are not clear from our confocal scans. Injections into the mushroom body calyces also provided no evidence that these structures receive projections from the ventral lobula.

Despite a conserved composition, interspecific and intersexual variation in the visual pathway extends to investment in visual neuropils

Volumetric data from segmented micro-CT scans allowed further quantitative volumetric comparisons of the main visual neuropils (Fig. 7). Two-way ANOVAs revealed significant interspecific differences for all four structures (lamina, F=4.617, d.f.=3, P=0.019; medulla, F_3=12. 543, P<0.001; lobula plate, F_3=11.806, P<0.001; lobula, F_3=14.180, P<0.001; optic lobe, F_3=11.192, P<0.001) with no sex or interaction effects found for any neuropils. Similar to our comparisons of eye volume, allometric analysis revealed all species effects to be the result of grade shifts in visual investment (lamina, Wald χ^2_3=17.86, P<0.001; medulla, Wald χ^2_3=43.42, P<0.001; lobula plate, Wald χ^2_3=39.27, P<0.001; lobula, Wald χ^2_3=40.80, P<0.001; optic lobe, Wald χ^2_3=30.68, P<0.001; Fig. 7B). For the medulla, lobula plate, lobula and optic lobe as a whole, significant pairwise comparisons commonly involved *G. morgane*, which consistently invested more in visual neuropil,

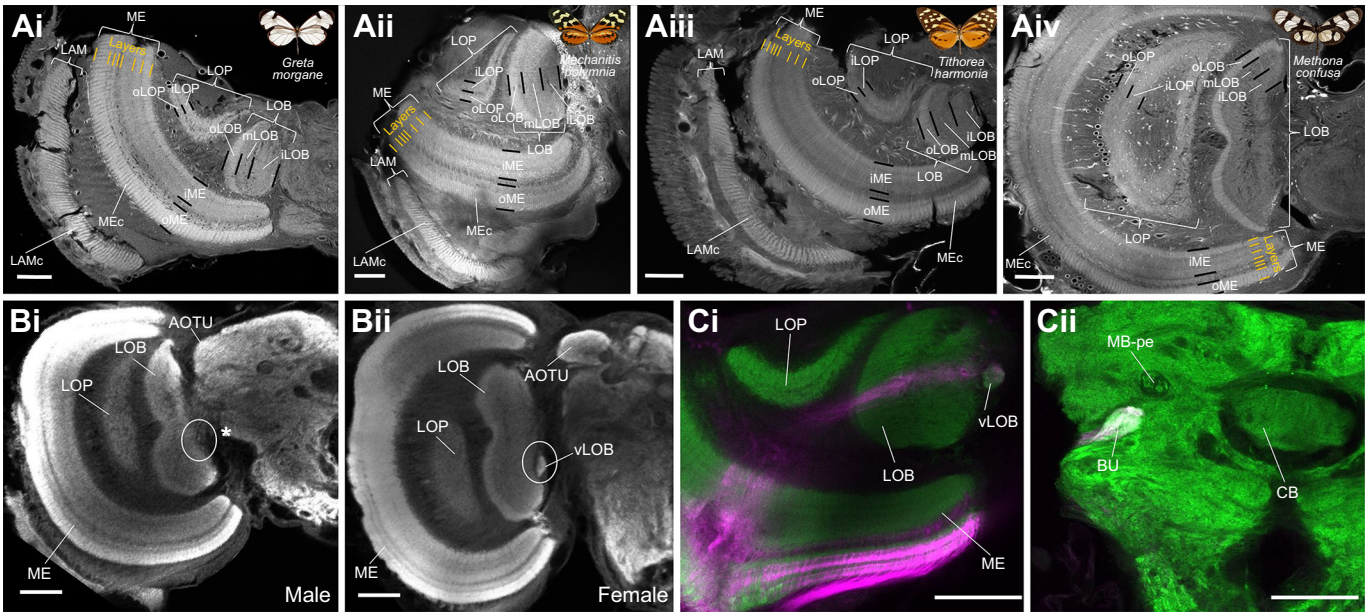

Fig. 6. Detailed neuroanatomy from immunostained brain samples (anti-allatostatin labelling: *n*=24, 54.17% female; dextran injections: *n*=24, 62.5% male). (A) Confocal images of anti-allatostatin labelled frontal vibratome sections (thickness, 80 μm) taken at approximately equivalent regions of the brain of *Greta morgane* (i), *Mechanitis polymnia* (ii), *Tithorea harmonia* (iii) and *Methona confusa* (iv). Divisions in the medulla (ME), lobula plate (LOP) and lobula (LOB) are shown using thick black lines, and finer-scale layering within the medulla is shown in orange. (B,C) Sexual dimorphism in the presence/absence of the ventral lobula, a butterfly-specific optic neuropil. (B) Confocal sections of anti-synapsin labelled wholemounts of a male (i) and female (ii) brain of *M. polymnia*. (C) Confocal section of a single female *G. morgane* brain, co-labelled against synapsin (green) and dextran injected neurons (magenta) originating from the medial optic lobe (i) and terminating in the bulb of the central brain (ii). All scale bars: 100 μm. LAM, lamina; LAMc, lamina cartridges; ME, medulla; Mec, medulla columns; iME: inner medulla; oME, outer medulla; LOP, lobula plate; iLOP, inner lobula plate; oLOP, outer lobula plate; LOB, lobula; iLOB, inner lobula; mLOB, middle lobula; oLOB, outer lobula; vLOB, ventral lobula; AOTU, anterior optic tubercle; BU, bulb; CB, central body; MB-pe, mushroom body peduncle.

Journal of Experimental Biology (2023) 226, jeb246423. doi:10.1242/jeb.246423

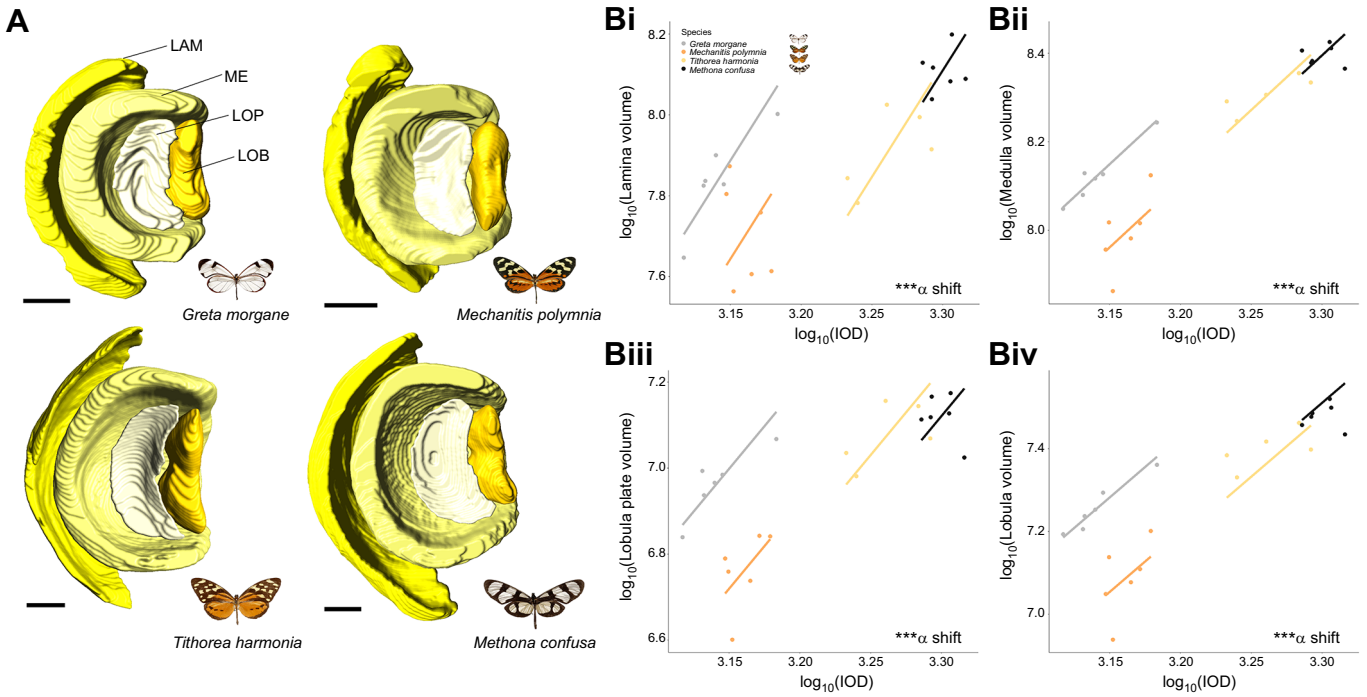

Fig. 7. Neuroanatomical variation in four ithomiine species from micro-CT measurements (*n*=23, 52.17% female). (A) Posterior surface reconstructions of the four main optic lobe neuropils (LAM, lamina; ME, medulla; LOP, lobula plate; LOB, lobula) for all four species shown to scale. Scale bar=200 µm. (B) Interspecific scaling relationships between interocular distance (IOD) and the lamina (i), medulla (ii), lobula plate (iii) and lobula (iv). An 'α shift' denotes a grade shift in the relationship between the two variables from our SMATR analysis. n.s. $P>0.05$, *$P<0.05$, **$P<0.01$, ***$P<0.001$.

for a given brain size, than the other three species, when accounting for IOD (Table S6).

A covariance matrix revealed significant correlations between the size of some of the optic neuropils and the eye (see Fig. S2). After controlling for this covariance and including species as an additional independent variable, the significant species effects remained for the eye (F=14.232, d.f.=3, P<0.001) and the lobula plate (F=3.530, d.f.=3, P=0.046). Therefore, interspecific differences in eye size appear, for the most part, to evolve in concert with investment in optic neuropils. Interestingly, interactions between functionally related neuropils appear to be obscuring sex effects, as significant sex differences in the medulla were revealed after controlling for this covariance (F=13.333, d.f.=1, P=0.003), with males investing in larger medullas. This is consistent with our observed patterns of sexually dimorphic eye investment (Fig. 5D), which also remained after controlling for this covariance (F=49.124, d.f.=1, P<0.001).

DISCUSSION

Specialisation in visual systems likely reflects selection pressures imposed by ecological needs, which act at the functional, physiological, anatomical and molecular level (e.g. Bartholomée et al., 2023; Gonzalez-Bellido et al., 2011; Hofmann et al., 2009; Huber et al., 1997; Scales and Butler, 2016; Sugawara et al., 2005; Zhao et al., 2009). By measuring physiological, anatomical and molecular variation in the eyes and visual neuropils of four closely butterfly species, we demonstrate multiple dimensions of variation in the visual system of Ithomiini. The 26-million-year-old adaptive radiation of these butterflies has been linked to microhabitat partitioning (Chazot et al., 2019; Elias et al., 2008; Hill, 2010), suggesting species are exposed to contrasting patterns of sensory information. By identifying aspects of the visual system that differ between species, we provide a foundation for future work linking variation in sensory ecology and sensory systems. Below, we discuss our results with this eco-evolutionary framework in mind.

Duplication and relaxed selection in UV opsins

Selection analyses on recovered visual opsin sequences revealed evidence of relaxation of selection. We found evidence of relaxed selection in the coding sequence of the UV-sensitive visual opsin in *G. morgane*, relative to nymphalid butterfly species living in open habitats (Fig. 2B; see Materials and Methods). Photosynthesising vegetation tends to absorb short wavelengths, particularly UV, making the light environment of the forest understory less rich in UV radiation than more exposed forest microhabitats (Endler, 1993; Théry, 2001). UV light is known to play a major role in butterfly interspecific and intraspecific communication and navigation (Briscoe et al., 2010; Brunton and Majerus, 1995; Froy et al., 2003; Sauman et al., 2005), but these cues may be less reliable for species occupying such densely shaded forest. Similar patterns were not observed for the B and LW-sensitive visual opsins. This relaxation of selective constraint might indicate a diminished role of UV-orientated behaviours in *G. morgane*, in comparison to its close relatives.

In contrast, we identified a duplication of the UV opsin in *T. harmonia*, making this the second independent duplication of this gene identified in butterflies (McCulloch et al., 2017; two additional duplications of this gene have been identified in non-papilionoid Lepidoptera, but with no known functional role, see Sondhi et al., 2021). In *Heliconius* butterflies, which exhibit an independent UV opsin duplication, the duplicated gene experienced positive selection in some lineages but relaxed selection in others, with the latter leading to pseudogenization or downregulated expression of this opsin in photoreceptor cells. Although it is tempting to link UV duplication to increased reliance on UV cues in *T. harmonia*, the duplicated copy also appears to have experienced relaxed selection,

which raises questions over its functionality (Fig. 2C). Nevertheless, our data illustrate the potential for divergent repertoires of opsin genes, and selection regimes governing their evolution, across Ithomiini. Larger-scale interspecific comparisons could provide opportunities to link this variation to preferences for different light environments.

Response to temporal and spatial light variation

Despite evidence of visual opsin conservation across all four species, photoreceptor sensitivity can also be shifted by changes in eye physiology. Our eyeshine images revealed a diversity of retinal mosaic patterns, caused by fixed combinations of photosensitive rhodopsins with additional screening pigments (Briscoe, 2008; Briscoe and Bernard, 2005; Stavenga and Arikawa, 2006). These screening pigments create the red-reflecting ommatidia seen in three of our four species (Fig. 3A), providing these species with an additional spectral channel for discriminating longer wavelengths (Belušič et al., 2021; Zaccardi et al., 2006).

Intraindividual variation between dorsal, frontal and ventral compound eye regions likely mirror spatial differences in sensory cue abundance and variability (Fig. 3A). Unlike frontal and ventral eye regions, dorsal facets have fewer or no red-reflecting ommatidia in their eyeshine. This indicates a specialisation for short wavelength sensitivity in dorsal ommatidia, which are exposed to a greater abundance of these wavelengths in downwelling light (Briscoe, 2008; Stalleicken et al., 2006). In addition, shorter ommatidia found within the dorsal region is a way of minimising self-screening for improved polarisation vision, which other butterflies have been shown to utilise for orientation and navigation, particularly within the dorsal rim area (Kinoshita and Arikawa, 2014; Labhart and Meyer, 1999; Meyer and Labhart, 1992; Nilsson et al., 1987; Reppert et al., 2004) (Fig. 5H). Although the dorsal rim area was not delineated in our image data, larger interommatidial angles in the dorsal area might hint that this region is optimised for enhanced contrast detection rather than improved visual acuity. The latter would be more beneficial in the frontal and ventral regions to optimise the localisation of hostplants, foodplants and mates (Bergman et al., 2021; Labhart and Meyer, 1999; Labhart et al., 2009; Land, 1989) (Fig. 5G). A greater abundance of downwelling light hitting the dorsal ommatidia (Stavenga, 2002) could also explain the narrower facets found within this region (Fig. 5I). In our ophthalmoscopy experiment, we found that the ventral region showed longer pupillary response times, which might reflect lower temporal variability in upwelling light intensity (Fig. 3D). Dorsal facing ommatidia must respond to rapid fluctuations in downwelling solar irradiance caused by gaps in the forest canopy, whereas frontal ommatidia must respond quickly to changes in other types of visual contrast, such as contrast variation created by optic flow when the animal is in flight to reduce motion blur. This role in stabilising visual processing during flight potentially explains the faster response times in these eye regions (Endler, 1993; Grittner et al., 2022; Palermo and Theobald, 2019; Théry, 2001). However, differences in pupillary kinetics between red- and yellow-reflecting ommatidia, which may further interact with variation in rhabdom and photoreceptor cross-sectional area, might also explain this result.

Comparing differences in frontal pupillary response time revealed that *G. morgane* and *M. polymnia* show slower responses times when exposed to a bright light stimulus following dark adaptation (Fig. 3B,C). Responding more slowly to fluctuations in light conditions may reflect a history of evolution within more homogeneous environments, and a strong preference for particular light conditions. Indeed, *G. morgane* tends to occupy constantly shaded forest understory (Elias and Joron, 2015; Willmott and Mallet, 2004), whereas *M. polymnia* might consistently occupy sunlit environments and therefore respond less rapidly to changes in light intensity than those from patchier forest, where *M. confusa* and *T. harmonia* are found. In addition, the longer, thinner wings of *M. confusa* are indicative of greater flight speeds (Hill, 2021), which might select for faster physiological responses owing to enhanced optic flow and contrast change during flight (Hill, 2021). However, we cannot rule out a degree of phylogenetic inertia in predicting these differences, given the closer relationships between these latter two species (Chazot et al., 2019). Larger species comparisons coupled with fine-scale ecological data (e.g. flight speed, light temporal variability, canopy cover) are required to disentangle the factors driving eye physiological variation, but the well-documented natural history of ithomiines (e.g. Beccaloni, 1997; Brown and Freitas, 1994; Willmott and Mallet, 2004) make them a prime model system for tackling these questions in future work.

Interspecific differences in eye and optic lobe structure

Across our four species, we identified extensive interspecific differences in optical and neural architecture which could not be explained solely by variation in overall head size or by evolutionary relatedness. Differences were observed for relative eye size, ommatidial length, facet diameter and the relative size of all four measured optic neuropils. In contrast, the lack of interspecific differences in interommatidial angle ($\Delta\Phi$) suggest that differences in visual acuity can be fully explained by differences in overall head size (as in Jander and Jander, 2002; Rutowski et al., 2009).

Larger relative eye size in *G. morgane* could, at least partially, be explained by enhanced ommatidial length in the frontal and ventral eye regions of this species (Fig. 5A,B). Longer rhabdoms provide a greater photoreceptive surface, and longer crystalline cones would enhance focal length. Together, this would optimise the eye for increased light sensitivity at greater distances (Greiner et al., 2004a; Warrant and McIntyre, 1993), which may be required in low-light conditions. The large relative volume of the lamina in *G. morgane* is consistent with the hypothesis that this species is enhancing either the signal-to-noise ratio for improved achromatic visual sensitivity and/or the amplitude of spectral opponency for improved colour vision (Fig. 7B; Matsushita et al., 2022; Sterling and Laughlin, 2015; Stöckl, 2022). The lamina is retinotopically organised, with lamina monopolar cells within neural cartridges receiving visual input from individual ommatidia (Fig. 6A). These lamina monopolar cells spatially integrate signals for enhancing light sensitivity (Greiner et al., 2005; Stöckl et al., 2016a, 2020). Larger lamina volumes observed in *G. morgane* therefore suggest that this species devotes greater neuronal resources to processing each visual pixel. Indeed, these patterns of investment are even more extreme in the remaining three optic neuropil, where *G. morgane* shows consistently larger visual neuropil than the other three species, controlling for head size (Fig. 7B). Therefore, increases in relative eye size appear to positively correlate with increases in neural processing (see also Garamszegi et al., 2002; Corral-López et al., 2017).

The relatively larger eyes, optic lobes and longer ommatidia of *G. morgane* might have evolved to enhance visual sensitivity, reflecting the shaded low-light forest understory where this species and its co-mimics are usually found (Elias et al., 2008; Willmott and Mallet, 2004; Willmott et al., 2017). In dense forest environments, overall illuminance is likely to be lower in comparison with the more sunlit

forest frequented by *M. polymnia*, *T. harmonia* and *M. confusa*, which all fly at higher elevations (Beccaloni, 1997; Elias et al., 2008; Endler, 1993; Hill, 2010). We note that these changes in relative investment may also arise to maintain functional visual sensitivity rather than increase it, given the constraints posed by a smaller head size (Rutowski et al., 2009). For example, the mean facet diameter (*D*) of *G. morgane* is similar to those of *M. confusa* and *T. harmonia*, despite these two species having a body size 7.12 and 4.13 times larger than that of *G. morgane* respectively (Fig. 5C). Hence, to overcome allometric size constraints and maintain visual performance, facet diameter must vary independently of head size.

Sexual dimorphism in the visual system

Patterns of eye sexual dimorphism within Ithomiini match previous findings from other Lepidoptera (e.g. Everett et al., 2012; Meyer-Rochow and Lau, 2008; Ziemba and Rutowski, 2000) and arthropods (e.g. Zeil, 1983) where relative eye size is larger in males. Other studies have proposed this to reflect greater visual sensitivity for male-limited visual behaviours such as the searching and localisation of potential mates and territorial defence (Bergman et al., 2021; Everett et al., 2012; McClure et al., 2019; Pliske, 1975; Rutowski, 2000) (Fig. 5D,F). This enhanced activity may also select for males to become more visually sensitive to the presence of predators (Everett et al., 2012). Unlike relative eye size, sexual dimorphism was not found for structures within the optic lobe, except for the medulla, but this was only revealed after controlling for covariance between optic neuropils (Fig. S2). Therefore, intersexual differences in visual ecology might promote changes in visual perception without downstream shifts in visual processing (e.g. by changing the number of lamina cartridges).

However, we also uncovered a rare case of dimorphism in the presence or absence of an apparently butterfly-specific optic neuropil – the ventral lobula (Fig. 6B). This small neuropil was absent in the 10 *G. morgane* and seven *M. polymnia* males we examined, but present in both sexes of *M. confusa* and *T. harmonia*. In other butterflies, the ventral lobula appears to be a relay centre directing visual projection neurons to the mushroom body calyx (Kinoshita et al., 2015; Couto et al., 2023). However, our own dextran neural tracing revealed no evidence of this pathway in ithomiines (Fig. 6C). Dextran fluorescence is instead detected in the bulb of the central brain, which might indicate that the ithomiine ventral lobula has different functional roles that, in the case of *G. morgane* and *M. polymnia*, presumably coordinates female-specific behaviours. In other insects, the bulb receives projections from the anterior optic tubercle and relays these signals to the ellipsoid body of the central complex, a collection of neuropils known to coordinate navigation and orientation behaviours (Hardcastle et al., 2021; Heinze et al., 2013; Lovick et al., 2017; Omoto et al., 2017). However, the small size of the ithomiine ventral lobula in comparison with other studied butterflies suggests overall lower functional performance in this neuropil (Montgomery and Ott, 2015; Wainwright and Montgomery, 2022). Nevertheless, this work provides striking evidence of neuroanatomical sexual dimorphism, further highlighting the lability of the nervous system to vary across short ecological and temporal scales.

Conclusions

Our qualitative and quantitative analysis reveals variation between and within species, which potentially reflects the different ecological conditions they occupy. Previous comparative work in a wild community of ithomiine butterflies mirrors these findings, having shown that small-scale ecological shifts can predict adaptive changes in other aspects of visual neuroanatomy (Wainwright and Montgomery, 2022). Our current work further integrates information on eye structure, physiology and molecular evolution. We present multiple lines of evidence that extensive visual system variation can exist within diverse insect radiations, hinting at the evolutionary lability of these systems to rapidly develop specialisations to distinct visual ecological niches, with selection potentially acting at the perceptual, processing and molecular level. We found physiological and anatomical differences between species, within species and within individuals, as well as evidence of gene duplications and relaxed selection in the visual opsins, and suggest various explanatory hypotheses for these results by linking our findings with knowledge of ithomiine natural history, behaviour and ecology. Larger comparative analyses across a greater number of species will enable the discrimination of adaptive processes from phylogenetic effects and repeated examples of microhabitat divergence and convergence within single communities make Ithomiini an ideal model system for identifying the ecological drivers of eye, brain and visual pigment diversification in the wild.

Acknowledgements

We are grateful to Alanna Kelly and Tom Pitman for support at the University of Bristol's Old Park Hill Greenhouse facility, and to Amaia Alcalde for assisting in butterfly rearing. We are also thankful to the University of Bristol's XTM Facility, Wolfson Bioimaging Facility and High Performance Computing Facility for micro-CT, confocal microscope and bioinformatics support, respectively. We also thank Nick Chazot for providing the phylogeny used in Fig. 1B, Antoine Couto for his assistance with the dextran tracing, and Jessica Foley for her support with aspects of the immunohistochemistry and microscopy protocols.

Competing interests

The authors declare no competing or financial interests.

Author contributions

Conceptualization: J.B.W., S.H.M.; Methodology: J.B.W., E.M.-S., E.A.B., F.C., M.J.H., S.H.M.; Validation: N.W.R., S.H.M.; Formal analysis: J.B.W.; Investigation: J.B.W., C.S., M.C., D.P., E.M.-S.; Resources: E.M.-S., E.A.B., F.C., M.J.H.; Data curation: J.B.W.; Writing - original draft: J.B.W.; Writing - review & editing: J.B.W., E.M.-S., E.A.B., F.C., M.J.H., N.W.R., S.H.M.; Visualization: J.B.W., E.A.B.; Supervision: N.W.R., S.H.M.; Project administration: J.B.W.; Funding acquisition: J.B.W., S.H.M.

Funding

This work was supported by the Natural Environment Research Council (GW4+ NERC DTP to J.B.W. and a NERC IRF NE/N014936/1 to S.H.M.), and the Air Force Research Laboratory/Air Force Office of Scientific Research (AFOSR) through the European Office of Aerospace Research and Development (EOARD) grant FA9550-18-1-7005. Open Access funding provided by University of Bristol. Deposited in PMC for immediate release.

Data availability

All raw data can be found in Tables S1–S3 and all opsin sequence alignment and gene tree files are available from the Dryad Digital Repository (Wainwright et al., 2023a): https://doi.org/10.5061/dryad.zcrjdfng3. All opsin sequences have been uploaded GenBank (accession IDs can be found in Table S1). All pseudopupil video recordings and micro-CT scans are available from Zenodo (Wainwright et al., 2023b): https://doi.org/10.5281/zenodo.8154379.

References

Arikawa, K., Pirih, P. and Stavenga, D. G. (2009). Rhabdom constriction enhances filtering by the red screening pigment in the eye of the eastern pale clouded yellow butterfly, *Colias erate* (Pieridae). *J. Exp. Biol.* **212**, 2057-2064. doi:10.1242/jeb.030692

Bartholomée, O., Dwyer, C., Tichit, P., Caplat, P., Baird, E. and Smith, H. G. (2023). Shining a light on species coexistence: visual traits drive bumblebee communities. *Proc. R. Soc. B Biol. Sci.* **290**, 20222548. doi:10.1098/rspb.2022.2548

Bates, H. W. (1862). XXXII. Contributions to an insect fauna of the Amazon valley (Lepidoptera: Heliconidae). *Trans. Linnean Soc. Lond.* **23**, 495-566. doi:10.1111/j.1096-3642.1860.tb00146.x

Beccaloni, G. W. (1997). Vertical stratification of ithomiine butterfly (Nymphalidae: Ithomiinae) mimicry complexes: the relationship between adult flight height and larva host-plant height. *Biol. J. Linn. Soc.* **62**, 313-341. doi:10.1111/j.1095-8312.1997.tb01629.x

Belušič, G., Ilić, M., Meglič, A. and Pirih, P. (2021). Red-green opponency in the long visual fibre photoreceptors of brushfoot butterflies (Nymphalidae). *Proc. R. Soc. B Biol. Sci.* **288**, 20211560. doi:10.1098/rspb.2021.1560

Bergman, M., Smolka, J., Nilsson, D.-E. and Kelber, A. (2021). Seeing the world through the eyes of a butterfly: visual ecology of the territorial males of *Pararge aegeria* (Lepidoptera: Nymphalidae). *J. Comp. Physiol. A* **207**, 701-713. doi:10.1007/s00359-021-01520-3

Borst, A. (2009). *Drosophila*'s view on insect vision. *Curr. Biol.* **19**, R36-R47. doi:10.1016/j.cub.2008.11.001

Brandt, R., Rohlfing, T., Rybak, J., Krofczik, S., Maye, A., Westerhoff, M., Hege, H.-C. and Menzel, R. (2005). Three-dimensional average-shape atlas of the honeybee brain and its applications. *J. Comp. Neurol.* **492**, 1-19. doi:10.1002/cne.20644

Briscoe, A. D. (2008). Reconstructing the ancestral butterfly eye: focus on the opsins. *J. Exp. Biol.* **211**, 1805-1813. doi:10.1242/jeb.013045

Briscoe, A. D. and Bernard, G. D. (2005). Eyeshine and spectral tuning of long wavelength-sensitive rhodopsins: no evidence for red-sensitive photoreceptors among five Nymphalini butterfly species. *J. Exp. Biol.* **208**, 687-696. doi:10.1242/jeb.01453

Briscoe, A. D. and Chittka, L. (2001). The evolution of color vision in insects. *Annu. Rev. Entomol.* **46**, 471-510. doi:10.1146/annurev.ento.46.1.471

Briscoe, A. D., Bybee, S. M., Bernard, G. D., Yuan, F., Sison-Mangus, M. P., Reed, R. D., Warren, A. D., Llorente-Bousquets, J. and Chiao, C.-C. (2010). Positive selection of a duplicated UV-sensitive visual pigment coincides with wing pigment evolution in *Heliconius* butterflies. *Proc. Natl Acad. Sci. USA* **107**, 3628-3633. doi:10.1073/pnas.0910085107

Brodrick, E. A., Roberts, N. W., Sumner-Rooney, L., Schlepütz, C. M. and How, M. J. (2020). Light adaptation mechanisms in the eye of the fiddler crab *Afruca tangeri*. *J. Comp. Neurol.* **529**, 616-634. doi:10.1002/cne.24973

Brown, K. S., , Jr and Freitas, A. V. L. (1994). Juvenile stages of Ithomiinae: overview and systematics (Lepidoptera: Nymphalidae). *Trop. Lepid.* **5**, 9-20.

Brunton, C. F. A. and Majerus, M. E. N. (1995). Ultraviolet colours in butterflies: intra- or inter-specific communication? *Proc. R. Soc. B Biol. Sci.* **260**, 199-204. doi:10.1098/rspb.1995.0080

Chazot, N., Willmott, K. R., Lamas, G., Freitas, A. V. L., Piron-Prunier, F., Arias, C. F., Mallet, J., De-Silva, D. L. and Elias, M. (2019). Renewed diversification following Miocene landscape turnover in a Neotropical butterfly radiation. *Glob. Ecol. Biogeogr.* **28**, 1118-1132. doi:10.1111/geb.12919

Corral-López, A., Garate-Olaizola, M., Buechel, S. D., Kolm, N. and Kotrschal, A. (2017). On the role of body size, brain size, and eye size in visual acuity. *Behav. Ecol. Sociobiol.* **71**, 179. doi:10.1007/s00265-017-2408-z

Couto, A., Wainwright, J. B., Morris, B. J. and Montgomery, S. H. (2020). Linking ecological specialisation to adaptations in butterfly brains and sensory systems. *Curr. Opin. Insect Sci.* **42**, 55-60. doi:10.1016/j.cois.2020.09.002

Couto, A., Young, F. J., Atzeni, D., Marty, S., Melo-Flórez, L., Hebberecht, L., Monllor, M., Neal, C., Cicconardi, F., Mcmillan, W. O. et al. (2023). Rapid expansion and visual specialisation of learning and memory centres in the brains of Heliconiini butterflies. *Nat. Commun.* **14**, 4024. doi:10.1038/s41467-023-39618-8

Cronin, T. W., Johnsen, S., Marshall, N. J. and Warrant, E. J. (2014). *Visual Ecology*. Princeton, NJ: Princeton University Press.

Dacke, M., Nordström, P., Scholtz, C. and Warrant, E. (2002). A specialised dorsal rim area for polarized light detection in the compound eye of the scarab beetle *Pachysoma striatum*. *J. Comp. Physiol. A* **188**, 211-216. doi:10.1007/s00359-002-0295-9

de Silva, D. L., Day, J. J., Elias, M., Willmott, K., Whinnett, A. and Mallet, J. (2010). Molecular phylogenetics of the neotropical butterfly subtribe Oleriina (Nymphalidae: Danainae: Ithomiini). *Mol. Phylogenet. Evol.* **55**, 1032-1041.

Elias, M. and Joron, M. (2015). Mimicry in *Heliconius* and Ithomiini butterflies: the profound consequences of an adaptation. *BIO Web Conf.* **4**, 0008. doi:10.1051/bioconf/20150400008

Elias, M., Gompert, Z., Jiggins, C. and Willmott, K. (2008). Mutualistic interactions drive ecological niche convergence in a diverse butterfly community. *PLoS Biol.* **6**, 2642-2649. doi:10.1371/journal.pbio.0060300

Endler, J. A. (1993). The color of light in forests and its implications. *Ecol. Monogr.* **63**, 1-27. doi:10.2307/2937121

Endler, J. A., Westcott, D. A., Madden, J. R. and Robson, T. (2005). Animal visual systems and the evolution of color patterns: sensory processing illuminates signal evolution. *Evolution* **59**, 1795-1818. doi:10.1111/j.0014-3820.2005.tb01827.x

Everett, A., Tong, X., Briscoe, A. D. and Monteiro, A. (2012). Phenotypic plasticity in opsin expression in a butterfly compound eye complements sex role reversal. *BMC Evol. Biol.* **12**, 232. doi:10.1186/1471-2148-12-232

Fain, G. L., Hardie, R. and Laughlin, S. B. (2010). Phototransduction and the evolution of photoreceptors. *Curr. Biol.* **20**, R114-R124. doi:10.1016/j.cub.2009.12.006

Farnworth, M. S. and Montgomery, S. H. (2022). Complexity of biological scaling suggests an absence of systematic trade-offs between sensory modalities in *Drosophila*. *Nat. Commun.* **13**, 2944. doi:10.1038/s41467-022-30579-y

Feuda, R., Marlétaz, F., Bentley, M. A. and Holland, P. W. H. (2016). Conservation, duplication, and divergence of five opsin genes in insect evolution. *Genome Biol. Evol.* **8**, 579-587. doi:10.1093/gbe/evw015

Franceschini, N. and Kirschfeld, K. (1971). Étude optique in vivo des éléments photorécepteurs dans l'oeil compose de *Drosophila*. *Kybernetik* **8**, 1-13. doi:10.1007/BF00270828

Frederiksen, R. and Warrant, E. J. (2008). Visual sensitivity in the crepuscular owl butterfly *Caligo memnon* and the diurnal blue morpho *Morpho peleides*: a clue to explain the evolution of nocturnal apposition eyes? *J. Exp. Biol.* **211**, 844-851. doi:10.1242/jeb.012179

Frentiu, F. D., Bernard, G. D., Cuevas, C. I., Sison-Mangus, M. P., Prudic, K. L. and Briscoe, A. D. (2007). Adaptive evolution of color vision as seen through the eyes of butterflies. *Proc. Natl. Acad. Sci. USA* **104**, 8634-8640. doi:10.1073/pnas.0701447104

Froy, O., Gotter, A. L., Casselman, A. L. and Reppert, S. M. (2003). Illuminating the circadian clock in monarch butterfly migration. *Science* **300**, 1303-1305. doi:10.1126/science.1084874

Garamszegi, L. Z., Møller, A. P. and Erritzøe, J. (2002). Coevolving avian eye size and brain size in relation to prey capture and nocturnality. *Proc. R. Soc. B Biol. Sci.* **269**, 961-967. doi:10.1098/rspb.2002.1967

Gompert, Z., Willmott, K. and Elias, M. (2011). Heterogeneity in predator microhabitat use and the maintenance of Müllerian mimetic diversity. *J. Theor. Biol.* **281**, 39-46. doi:10.1016/j.jtbi.2011.04.024

Gonzalez-Bellido, P. T., Wardill, T. J. and Juusola, M. (2011). Compound eyes and retinal information processing in miniature dipteran species match their specific ecological demands. *Proc. Natl Acad. Sci. USA* **108**, 4224-4229. doi:10.1073/pnas.1014438108

Gouy, M., Tannier, E., Comte, N. and Parsons, D. P. (2021). Seaview Version 5: a multiplatform software for multiple sequence alignment, molecular phylogenetic analyses, and tree reconciliation. *Methods Mol. Biol.* **1198**, 241-260. doi:10.1007/978-1-0716-1036-7_15

Greiner, B. (2006). Adaptations for nocturnal vision in insect apposition eyes. *Int. Rev. Cytol.* **250**, 1-46. doi:10.1016/S0074-7696(06)50001-4

Greiner, B., Ribi, W. A. and Warrant, E. J. (2004a). Retinal and optical adaptations for nocturnal vision in the halictid bee *Megalopta genalis*. *Cell Tissue Res.* **316**, 377-390. doi:10.1007/s00441-004-0883-9

Greiner, B., Ribi, W. A., Wcislo, W. T. and Warrant, E. J. (2004b). Neural organisation in the first optic ganglion of the nocturnal bee *Megalopta genalis*. *Cell Tissue Res.* **318**, 429-437. doi:10.1007/s00441-004-0945-z

Greiner, B., Ribi, W. A. and Warrant, E. J. (2005). A neural network to improve dim-light vision? Dendritic fields of first-order interneurons in the nocturnal bee *Megalopta genalis*. *Cell Tissue Res.* **322**, 313-320. doi:10.1007/s00441-005-0034-y

Grittner, R., Baird, E. and Stöckl, A. (2022). Spatial tuning of translational optic flow responses in hawkmoths of varying body size. *J. Comp. Physiol. A* **208**, 279-296. doi:10.1007/s00359-021-01530-1

Hamanaka, Y., Kinoshita, M., Homberg, U. and Arikawa, K. (2012). Immunocytochemical localization of amines and GABA in the optic lobe of the butterfly, *Papilio xuthus*. *PLoS ONE* **7**, e41109. doi:10.1371/journal.pone.0041109

Hardcastle, B. J., Omoto, J. J., Kandimalla, P., Nguyen, B.-C. M., Keleş, M. F., Boyd, N. K., Hartenstein, V. and Frye, M. A. (2021). A visual pathway for skylight polarization processing in *Drosophila*. *eLife* **10**, e63225. doi:10.7554/eLife.63225

Hebberecht, L., Wainwright, J. B., Thompson, C., Kershenbaum, S., Mcmillan, W. O. and Montgomery, S. H. (2023). Plasticity and genetic effects contribute to different axes of neural divergence in a community of mimetic *Heliconius* butterflies. *J. Evol. Biol.* **36**, 1116-1132. doi:10.1111/jeb.14188

Heinze, S. and Reppert, S. M. (2011). Sun compass integration of skylight cues in migratory monarch butterflies. *Neuron* **69**, 345-358. doi:10.1016/j.neuron.2010.12.025

Heinze, S. and Reppert, S. M. (2012). Anatomical basis of sun compass navigation. I: The general layout of the monarch butterfly brain. *J. Comp. Neurol.* **520**, 1599-1628. doi:10.1002/cne.23054

Heinze, S., Florman, J., Asokaraj, S., El Jundi, B. and Reppert, S. M. (2013). Anatomical basis of sun compass navigation. II: the neuronal composition of the central complex of the monarch butterfly. *J. Comp. Neurol.* **521**, 267-298. doi:10.1002/cne.23214

Hill, R. I. (2010). Habitat segregation among mimetic ithomiine butterflies (Nymphalidae). *Evol. Ecol.* **24**, 273-285. doi:10.1007/s10682-009-9305-5

Hill, R. I. (2021). Convergent flight morphology among Müllerian mimic mutualists. *Evolution* **75**, 2460-2479. doi:10.1111/evo.14331

Hoang, D. T., Chernomor, O., Von Haeseler, A., Minh, B. Q. and Vinh, L. S. (2018). UFBoot2: improving the ultrafast bootstrap approximation. *Mol. Biol. Evol.* **35**, 518-522. doi:10.1093/molbev/msx281

Hofmann, C. M., O'Quin, K. E., Marshall, N. J., Cronin, T. W., Seehausen, O. and Carleton, K. L. (2009). The eyes have it: regulatory and structural changes both

underlie cichlid visual pigment diversity. *PLoS Biol.* **7**, e1000266. doi:10.1371/journal.pbio.1000266
Huber, R., van Staaden, M. J., Kaufman, L. S. and Liem, K. F. (1997). Microhabitat use, trophic patterns and the evolution of brain structure in African cichlids. *Brain Behav. Evol.* **50**, 167-182. doi:10.1159/000113330
Jander, U. and Jander, R. (2002). Allometry and resolution of bee eyes (Apoidea). *Arthropod. Struct. Dev.* **30**, 179-193. doi:10.1016/S1467-8039(01)00035-4
Kall, L., Krogh, A. and Sonnhammer, E. L. L. (2007). Advantages of combined transmembrane topology and signal peptide prediction–the Phobius web server. *Nucleic Acids Res.* **35**, 429-432. doi:10.1093/nar/gkm256
Kalyaanamoorthy, S., Minh, B. Q., Wong, T. K. F., Von Haeseler, A. and Jermiin, L. S. (2017). ModelFinder: fast model selection for accurate phylogenetic estimates. *Nat. Methods* **14**, 587-589. doi:10.1038/nmeth.4285
Kinoshita, M. and Arikawa, K. (2014). Color and polarization vision in foraging *Papilio*. *J. Comp. Physiol. A* **200**, 513-526. doi:10.1007/s00359-014-0903-5
Kinoshita, M., Shimohigasshi, M., Tominaga, Y., Arikawa, K. and Homberg, U. (2015). Topographically distinct visual and olfactory inputs to the mushroom body in the swallowtail butterfly, *Papilio xuthus*. *J. Comp. Neurol.* **523**, 162-182. doi:10.1002/cne.23674
Klagges, B. R. E., Heimbeck, G., Godenschwege, T. A., Hofbauer, A., Pflugfelder, G. O., Reifegerste, R., Reisch, D., Schaupp, M., Buchner, S. and Buchner, E. (1996). Invertebrate synapsins: a single gene codes for several isoforms in *Drosophila*. *J. Neurosci.* **16**, 3154-3165. doi:10.1523/JNEUROSCI.16-10-03154.1996
Kosakovsky Pond, S. L., Murrell, B., Fourment, M., Frost, S. D. W., Delport, W. and Scheffler, K. (2011). A random effects branch-site model for detecting episodic diversifying selection. *Mol. Biol. Evol.* **28**, 3033-3043. doi:10.1093/molbev/msr125
Kosakovsky Pond, S. L., Poon, A. F. Y., Velazquez, R., Weaver, S., Hepler, N. L., Murrell, B., Shank, S. D., Magalis, B. R., Bouvier, D., Nekrutenko, A. et al. (2020). HyPhy 2.5—a customizable platform for evolutionary hypothesis testing using phylogenies. *Mol. Biol. Evol.* **37**, 295-299. doi:10.1093/molbev/msz197
Kreissl, S., Strasser, C. and Galizia, C. G. (2010). Allatostatin immunoreactivity in the honeybee brain. *J. Comp. Neurol.* **518**, 1391-1417. doi:10.1002/cne.22343
Kruska, D. C. T. (2005). On the evolutionary significance of encephalization in some eutherian mammals: effects of adaptive radiation, domestication, and fertilization. *Brain Behav. Evol.* **65**, 73-108. doi:10.1159/000082979
Labhart, T. and Meyer, E. P. (1999). Detectors for polarized skylight in insects: a survey of ommatidial specializations in the dorsal rim area of the compound eye. *Microsc. Res. Tech.* **47**, 368-379. doi:10.1002/(SICI)1097-0029(19991215)47:6<368::AID-JEMT2>3.0.CO;2-Q
Labhart, T., Baumann, F. and Bernard, G. D. (2009). Specialized ommatidia of the polarization-sensitive dorsal rim area in the eye of monarch butterflies have non-functional reflecting tapeta. *Cell Tissue Res.* **338**, 391-400. doi:10.1007/s00441-009-0886-7
Land, M. F. (1989). Variations in the structure and design of compound eyes. In *Facets of Vision* (ed. D. G. Stavenga and R. C. Hardie), pp. 90-111. Berlin, Heidelberg: Springer.
Land, M. F. (1997). Visual acuity in insects. *Annu. Rev. Entomol.* **42**, 147-177. doi:10.1146/annurev.ento.42.1.147
Land, M. F. and Nilsson, D. E. (2012). *Animal Eyes*. Oxford: Oxford University Press.
Laughlin, S. B., de Rutyer van Steveninck, R. R. and Anderson, J. C. (1998). The metabolic cost of neural information. *Nat. Neurosci.* **1**, 36-41. doi:10.1038/236
Lehrer, M. (1998). Looking all around: honeybees use different cues in different eye regions. *J. Exp. Biol.* **201**, 3275-3292. doi:10.1242/jeb.201.24.3275
Lin, T.-Y., Luo, J., Shinomiya, K., Ting, C.-Y., Lu, Z., Meinertzhagen, I. A. and Lee, C.-H. (2015). Mapping chromatic pathways in the *Drosophila* visual system. *J. Comp. Physiol.* **524**, 213-227. doi:10.1002/cne.23857
Lin, C., Hoving, H.-J. T., Cronin, T. W. and Osborn, K. J. (2021). Strange eyes, stranger brains: exceptional diversity of optic lobe organization in midwater crustaceans. *Proc. R. Soc. B Biol. Sci.* **288**, 20210216. doi:10.1098/rspb.2021.0216
Lovick, J. K., Omoto, J. J., Ngo, K. T. and Hartenstein, V. (2017). Development of the anterior visual input pathway to the *Drosophila* central complex. *J. Comp. Neurol.* **525**, 3458-3475. doi:10.1002/cne.24277
Lythgoe, J. N. (1979). *The Ecology of Vision*. Oxford: Clarendon.
Mappes, M. and Homberg, U. (2004). Behavioral analysis of polarization vision in tethered flying locusts. *J. Comp. Physiol. A* **190**, 61-68. doi:10.1007/s00359-003-0473-4
Matsushita, A., Stewart, F., Ilić, M., Chen, P.-J., Wakita, D., Miyazaki, N., Murata, K., Kinoshita, M., Belušič, G. and Arikawa, K. (2022). Connectome of the lamina reveals the circuit for early color processing in the visual pathway of a butterfly. *Curr. Biol.* **32**, 2291-2299.e3. doi:10.1016/j.cub.2022.03.066
McClure, M., Mahrouche, L., Houssin, C., Monllor, M., Le Poul, Y., Frérot, B., Furtos, A. and Elias, M. (2019). Does divergent selection predict the evolution of mate preference and reproductive isolation in the tropical butterfly genus *Melinaea* (Nymphalidae: Ithomiini)? *J. Anim. Ecol.* **88**, 940-952. doi:10.1111/1365-2656.12975
McCulloch, K. J., Yuan, F., Zhen, Y., Aardema, M. L., Smith, G., Llorente-Bousquets, J., Andolfatto, P. and Briscoe, A. D. (2017). Sexual dimorphism and retinal mosaic diversification following the evolution of a violet receptor in butterflies. *Mol. Biol. Evol.* **34**, 2271-2284. doi:10.1093/molbev/msx163
Meyer, E. P. and Labhart, T. (1992). Morphological specializations of dorsal rim ommatidia in the compound eye of dragonflies and damselflies (Odonata). *Cell Tissue Res.* **272**, 17-22. doi:10.1007/BF00323566
Meyer-Rochow, V. B. and Lau, T. F. S. (2008). Sexual dimorphism in the compound eye of the moth *Operophtera brumata* (Lepidoptera, Geometridae). *Invertebr. Biol.* **127**, 201-216. doi:10.1111/j.1744-7410.2008.00131.x
Montgomery, S. H. and Merrill, R. M. (2017). Divergence in brain composition during the early stages of ecological specialization in *Heliconius* butterflies. *J. Evol. Biol.* **30**, 571-582. doi:10.1111/jeb.13027
Montgomery, S. H. and Ott, S. R. (2015). Brain composition in *Godyris zavaleta*, a diurnal butterfly, reflects an increased reliance on olfactory information. *J. Comp. Neurol.* **523**, 869-891. doi:10.1002/cne.23711
Montgomery, S. H., Merrill, R. M. and Ott, S. R. (2016a). Brain composition in *Heliconius* butterflies, posteclosion growth and experience-dependent neuropil plasticity. *J. Comp. Neurol.* **524**, 1747-1769. doi:10.1002/cne.23993
Montgomery, S. H., Mundy, N. I. and Barton, R. A. (2016b). Brain evolution and development: adaptation, allometry and constraint. *Proc. R. Soc. B Biol. Sci.* **283**, 20160433. doi:10.1098/rspb.2016.0433
Montgomery, S. H., Rossi, M., Mcmillan, W. O. and Merrill, R. M. (2021). Neural divergence and hybrid disruption between ecologically isolated *Heliconius* butterflies. *Proc. Natl. Acad. Sci. USA* **118**, e2015102118. doi:10.1073/pnas.2015102118
Moran, D., Softley, R. and Warrant, E. J. (2015). The energetic cost of vision and the evolution of eyeless Mexican cavefish. *Sci. Adv.* **1**, e1500363. doi:10.1126/sciadv.1500363
Morris, B. J., Couto, A., Aydin, A. and Montgomery, S. H. (2021). Re-emergence and diversification of a specialized antennal lobe morphology in ithomiine butterflies. *Evolution* **75**, 3191-3202. doi:10.1111/evo.14324
Müller, F. (1879). *Ituna* and *Thyridia*; a remarkable case of mimicry in butterflies. *Trans. Entomol. Society Lond.* **1879**, xx-xxix.
Narendra, A., Alkaladi, A., Raderschall, C. A., Robson, S. K. A. and Ribi, W. A. (2013). Compound eye adaptations for diurnal and nocturnal lifestyle in the intertidal ant, *Polyrhachis sokolova*. *PLoS ONE* **8**, e76015. doi:10.1371/journal.pone.0076015
Nilsson, D.-E. and Smolka, J. (2021). Quantifying biologically essential aspects of environmental light. *J. R. Soc. Interface* **18**, 20210184. doi:10.1098/rsif.2021.0184
Nilsson, D.-E., Labhart, T. and Meyer, E. P. (1987). Photoreceptor design and optical properties affecting polarization sensitivity in ants and crickets. *J. Comp. Physiol. A* **161**, 645-658. doi:10.1007/BF00605006
Nilsson, D.-E., Land, M. F. and Howard, J. (1988). Optics of the butterfly eye. *J. Comp. Physiol. A* **162**, 341-366. doi:10.1007/BF00606122
Nilsson, D.-E., Smolka, J. and Bok, M. (2022). The vertical light-gradient and its potential impact on animal distribution and behavior. *Front. Ecol. Evol.* **10**, 951328. doi:10.3389/fevo.2022.951328
Niven, J. E. and Laughlin, S. B. (2008). Energy limitation as a selective pressure on the evolution of sensory systems. *J. Exp. Biol.* **211**, 1792-1804. doi:10.1242/jeb.017574
Niven, J. E., Anderson, J. C. and Laughlin, S. B. (2007). Fly photoreceptors demonstrate energy-information trade-offs in neural coding. *PLoS Biol.* **5**, e116. doi:10.1371/journal.pbio.0050116
Omasits, U., Ahrens, C. H., Müller, S. and Wollscheid, B. (2014). Protter: interactive protein feature visualization and integration with experimental proteomic data. *Bioinformatics* **30**, 884-886. doi:10.1093/bioinformatics/btt607
Omoto, J. J., Keleş, M. F., Nguyen, B.-C. M., Bolanos, C., Lovick, J. K., Frye, M. A. and Hartenstein, V. (2017). Visual input to the *Drosophila* central complex by developmentally and functionally distinct neuronal populations. *Curr. Biol.* **27**, 1098-1110. doi:10.1016/j.cub.2017.02.063
Osorio, D., Averof, M. and Bacon, J. P. (1995). Arthropod evolution: great brains, beautiful bodies. *Trends Ecol. Evol.* **10**, 449-454. doi:10.1016/S0169-5347(00)89178-8
Ott, S. R. (2008). Confocal microscopy in large insect brains: zinc-formaldehyde fixation improves synapsin immunostaining and preservation of morphology in whole-mounts. *J. Neurosci. Methods* **172**, 220-230. doi:10.1016/j.jneumeth.2008.04.031
Palermo, N. and Theobald, J. (2019). Fruit flies increase attention to their frontal visual field during fast forward optic flow. *Biol. Lett.* **15**, 20180767. doi:10.1098/rsbl.2018.0767
Pliske, T. E. (1975). Courtship behavior and use of chemical communication by males of certain species of ithomiine butterflies (Nymphalidae: Lepidoptera). *Ann. Entomol. Soc. Am.* **68**, 935-942. doi:10.1093/aesa/68.6.935
Qiu, X., Vanhoutte, K. J. A., Stavenga, D. G. and Arikawa, K. (2002). Ommatidial heterogeneity in the compound eye of the male small white butterfly, *Pieris rapae crucivora*. *Cell Tissue Res.* **307**, 371-379. doi:10.1007/s00441-002-0517-z
Ranwez, V., Douzery, E. J. P., Cambon, C., Chantret, N. and Delsuc, F. (2018). MACSE v2: toolkit for the alignment of coding sequences accounting for

frameshifts and stop codons. *Mol. Biol. Evol.* **35**, 2582-2584. doi:10.1093/molbev/msy159
Reppert, S. M., Zhu, H. and White, R. H. (2004). Polarized light helps monarch butterflies navigate. *Curr. Biol.* **14**, 155-158. doi:10.1016/j.cub.2003.12.034
Rutowski, R. L. (2000). Variation of eye size in butterflies: inter- and intraspecific patterns. *J. Zool.* **252**, 187-195. doi:10.1111/j.1469-7998.2000.tb00614.x
Rutowski, R. L., Gislén, L. and Warrant, E. J. (2009). Visual acuity and sensitivity increase allometrically with body size in butterflies. *Arthropod. Struct. Dev.* **38**, 91-100. doi:10.1016/j.asd.2008.08.003
Sauman, I., Briscoe, A. D., Zhu, H., Shi, D., Froy, O., Stalleicken, J., Yuan, Q., Casselman, A. and Reppert, S. M. (2005). Connecting the navigational clock to sun compass input in monarch butterfly brain. *Neuron* **46**, 457-467. doi:10.1016/j.neuron.2005.03.014
Scales, J. A. and Butler, M. A. (2016). The relationship between microhabitat use, allometry and functional variation in the eyes of Hawaiian *Megalagrion* damselflies. *Funct. Ecol.* **30**, 356-368. doi:10.1111/1365-2435.12479
Schindelin, J., Arganda-Carreras, I., Frise, E., Kaynig, V., Longair, M., Pietzsch, T., Preibisch, S., Rueden, C., Saalfeld, S., Schmid, B. et al. (2012). Fiji: an open-source platform for biological-image analysis. *Nat. Methods* **9**, 676-682. doi:10.1038/nmeth.2019
Seymoure, B. M., Mcmillan, W. O. and Rutowski, R. (2015). Peripheral eye dimensions in longwing (*Heliconius*) butterflies vary with body size and sex but not light environment nor mimicry ring. *J. Res. Lepidoptera* **48**, 83-92. doi:10.5962/p.266475
Sinakevitch, I., Douglass, J. K., Scholtz, G., Loesel, R. and Strausfeld, N. J. (2003). Conserved and convergent organization in the optic lobes of insects and isopods, with reference to other crustacean taxa. *J. Comp. Neurol.* **467**, 150-172. doi:10.1002/cne.10925
Sivasubramanian, P. and Sood, P. P. (2003). Allatostatin-like immunoreactivity in the optic lobe of the fly *Sarophaga bullata*. *Cell. Mol. Biol. (Noisy-le-grand)* **49**, 641-644.
Slater, G. S. C. and Birney, E. (2005). Automated generation of heuristics for biological sequence comparison. *BMC Bioinformatics* **6**, 1-11. doi:10.1186/1471-2105-6-31
Smith, D. B., Bernhardt, G., Raine, N. E., Abel, R. L., Sykes, D., Ahmned, F., Pedroso, I. and Gill, R. J. (2016). Exploring miniature insect brains using micro-CT scanning techniques. *Sci. Rep.* **6**, 21768. doi:10.1038/srep21768
Somanathan, H., Kelber, A., Borges, R. M., Wallén, R. and Warrant, E. J. (2009). Visual ecology of Indian carpenter bees II: adaptations of eyes and ocelli to nocturnal and diurnal lifestyles. *J. Comp. Physiol. A* **195**, 571-583. doi:10.1007/s00359-009-0432-9
Sondhi, Y., Ellis, E. A., Bybee, S. M., Theobald, J. C. and Kawahara, A. Y. (2021). Light environment drives evolution of color vision genes in butterflies and moths. *Commun. Biol.* **4**, 177. doi:10.1038/s42003-021-01688-z
Stalleicken, J., Labhart, T. and Mouritsen, H. (2006). Physiological characterization of the compound eye in monarch butterflies with focus on the dorsal rim area. *J. Comp. Physiol. A* **192**, 321-331. doi:10.1007/s00359-005-0073-6
Stansbury, M. S. and Moczek, A. P. (2013). The evolvability of arthropods. In: *Arthropod Biology and Evolution: Molecules, Development, Morphology* (ed. A. Minelli, G. Boxshall, G. Fusco), pp. 479-493. Berlin, Heidelberg: Springer-Verlag.
Stavenga, D. G. (1979). Pseudopupils of compound eyes. In: *Handbook of Sensory Physiology*, Vol. VII/6A (ed. H. Autrum), pp. 357-439. Berlin, Heidelberg, New York: Springer.
Stavenga, D. G. (1992). Eye regionalization and spectral tuning of retinal pigments in insects. *Trends Neurosci.* **15**, 213-218. doi:10.1016/0166-2236(92)90038-A
Stavenga, D. G. (2002). Reflections on colourful ommatidia of butterfly eyes. *J. Exp. Biol.* **205**, 1077-1085. doi:10.1242/jeb.205.8.1077
Stavenga, D. G. and Arikawa, K. (2006). Evolution of color and vision of butterflies. *Arthropod. Struct. Dev.* **35**, 307-318. doi:10.1016/j.asd.2006.08.011
Stavenga, D. G., Numan, J. A. J., Tinbergen, J. and Kuiper, J. W. (1977). Insect pupil mechanisms. II. Pigment migration in retinula cells of butterflies. *J. Comp. Physiol. A* **113**, 73-93. doi:10.1007/BF00610454
Stavenga, D. G., Kinoshita, M., Yang, E.-C. and Arikawa, K. (2001). Retinal regionalization and heterogeneity of butterfly eyes. *Naturwissenschaften* **88**, 477-481. doi:10.1007/s001140100268
Sterling, P. and Laughlin, S. (2015). *Principles of Neural Design*. Cambridge, MA: MIT Press.
Stöckl, A. (2022). Connectomics: from form to function in butterfly colour vision. *Curr. Biol.* **32**, 457-481. doi:10.1016/j.cub.2022.04.026
Stöckl, A., Heinze, S., Charalabidis, A., el Jundi, B., Warrant, E. and Kelber, A. (2016a). Differential investment in visual and olfactory brain areas reflects behavioural choices in hawk moths. *Sci. Rep.* **6**, 26041. doi:10.1038/srep26041
Stöckl, A. L., Ribi, W. A. and Warrant, E. J. (2016b). Adaptations for nocturnal and diurnal vision in the hawkmoth lamina. *J. Comp. Neurol.* **524**, 160-175. doi:10.1002/cne.23832
Stöckl, A. L., O'Carroll, D. C. and Warrant, E. J. (2020). Hawkmoth lamina monopolar cells act as dynamic spatial filters to optimize vision at different light levels. *Sci. Adv.* **6**, eaaz8645. doi:10.1126/sciadv.aaz8645
Strausfeld, N. J. and Nässel, D. R. (1980). Neuroarchitecture of brain regions that subserve the compound eyes of crustacea and insects. In: *Handbook of Sensory Physiology* (ed. H. Autrum), pp. 102-112. Berlin: Springer-Verlag.
Striedter, G. F. (2005). *Principles of Brain Evolution*. Sunderland: Sinauer Associates.
Sugawara, T., Terai, Y., Imai, H., Turner, G. F., Koblmüller, S., Sturmbauer, C., Shichida, Y. and Okada, N. (2005). Parallelism of amino acid changes at the RH1 affecting spectral sensitivity among deep-water cichlids from lakes Tanganyika and Malawi. *Proc. Natl. Acad. Sci. USA* **102**, 5448-5453. doi:10.1073/pnas.0405302102
Swart, P., Wicklein, M., Sykes, D., Ahmed, F. and Krapp, H. G. (2016). A quantitative comparison of micro-CT preparations in Dipteran flies. *Sci. Rep.* **6**, 39380. doi:10.1038/srep39380
Sylvester, J. B., Pottin, K. and Streelman, J. T. (2011). Integrated brain diversification along the early neuraxes. *Brain Behav. Evol.* **78**, 237-247. doi:10.1159/000329840
Terakita, A. (2005). The opsins. *Genome Biol.* **6**, 213. doi:10.1186/gb-2005-6-3-213
Théry, M. (2001). Forest light and its influence on habitat selection. *Plant Ecol.* **153**, 251-261. doi:10.1023/A:1017592631542
Trifinopoulos, J., Nguyen, L.-T., von Haeseler, A. and Minh, B. Q. (2016). Q-IQ-TREE: a fast online phylogenetic tool for maximum likelihood analysis. *Nucleic Acids Res.* **44**, 232-235. doi:10.1093/nar/gkw256
Turlure, C., Schtickzelle, N., van Dyck, H., Seymoure, B. and Rutowski, R. (2016). Flight morphology, compound eye structure and dispersal in the bog and the cranberry fritillary butterflies: an inter- and intraspecific comparison. *PLoS ONE* **11**, e0158073. doi:10.1371/journal.pone.0158073
Wainwright, J. B. and Montgomery, S. H. (2022). Neuroanatomical shifts mirror patterns of ecological divergence in three diverse clades of mimetic butterflies. *Evolution* **76**, 1806-1820. doi:10.1111/evo.14547
Wainwright, J. B., Schofield, C., Conway, M., Phillips, D., Martin-Silverstone, E., Brodrick, E. A., Cicconardi, F., How, M. J., Roberts, N. W. and Montgomery, S. H. (2023a). Opsin data from: Multiple axes of visual system diversity in Ithomiini, an ecologically diverse tribe of mimetic butterflies. [Dataset]. Dryad. https://doi.org/10.5061/dryad.zcrjdfng3
Wainwright, J. B., Schofield, C., Conway, M., Phillips, D., Martin-Silverstone, E., Brodrick, E. A., Cicconardi, F., How, M. J., Roberts, N. W. and Montgomery, S. H. (2023b). Multiple axes of visual system diversity in Ithomiini, an ecologically diverse tribe of mimetic butterflies – Ophthalmoscope video recordings and microCT scansm. Zenodo Digital Repository. doi:10.5281/zenodo.8154379
Warrant, E. J. (2001). The design of compound eyes and the illumination of natural habitats. In: *Ecology of Sensing* (ed. F. G. Barth and A. Schmid), pp. 187-213. Berlin, Heidelberg: Springer.
Warrant, E. J. (2017). The remarkable visual capacities of nocturnal insects: vision at the limits with small eyes and tiny brains. *Philos. Trans. R. Soc. B Biol. Sci.* **372**, 20160063. doi:10.1098/rstb.2016.0063
Warrant, E. J. and Mcintyre, P. D. (1993). Arthropod eye design and the physical limits to spatial resolving power. *Prog. Neurobiol.* **40**, 413-461. doi:10.1016/0301-0082(93)90017-M
Warrant, E. J., Kelber, A., Gislén, A., Greiner, B., Ribi, W. and Wcislo, W. T. (2004). Nocturnal vision and landmark orientation in a tropical halictid bee. *Curr. Biol.* **14**, 1309-1318. doi:10.1016/j.cub.2004.07.057
Warton, D. I., Duursma, R. A., Falster, D. S. and Taskinen, S. (2012). smatr 3 – an R package for estimation and inference about allometric lines. *Methods Ecol. Evol.* **3**, 257-259. doi:10.1111/j.2041-210X.2011.00153.x
Waterhouse, A., Bertoni, M., Bienert, S., Studer, G., Tauriello, G., Gumienny, R., Heer, F. T., de Beer, T. A. P., Rempfer, C., Bordoli, L. et al. (2018). SWISS-MODEL: homology modelling of protein structures and complexes. *Nucleic Acids Res.* **46**, W296-W303. doi:10.1093/nar/gky427
Wertheim, J. O., Murrell, B., Smith, M. D., Kosakovsky Pond, S. L. and Scheffler, K. (2015). RELAX: detecting relaxed selection in a phylogenetic framework. *Mol. Biol. Evol.* **32**, 820-832. doi:10.1093/molbev/msu400
White, R. H., Xu, H., Münch, T. A., Bennett, R. R. and Grable, E. A. (2003). The retina of *Manduca sexta*: rhodopsin expression, the mosaic of green-, blue- and UV-sensitive photoreceptors, and regional specialization. *J. Exp. Biol.* **206**, 3337-3348. doi:10.1242/jeb.00571
Willmott, K. R. and Mallet, J. (2004). Correlations between adult mimicry and larval host plants in ithomiine butterflies. *Proc. R. Soc. B Biol. Sci.* **271**, 266-269. doi:10.1098/rsbl.2004.0184
Willmott, K. R., Willmott, J. C. R., Elias, M. and Jiggins, C. D. (2017). Maintaining mimicry diversity: optimal warning colour patterns differ among microhabitats in Amazonian clearwing butterflies. *Proc. R. Soc. B Biol. Sci.* **284**, 20170744. doi:10.1098/rspb.2017.0744
Yack, J. E., Johnson, S. E., Brown, S. G. and Warrant, E. J. (2007). The eyes of *Macrosoma* sp. (Lepidoptera: Hedyloidea): a nocturnal butterfly with superposition optics. *Arthropod. Struct. Dev.* **36**, 11-22. doi:10.1016/j.asd.2006.07.001
Yilmaz, A., Hempel De Ibarra, N. and Kelber, A. (2022). High diversity of arthropod colour vision: from genes to ecology. *Philos. Trans. R. Soc. B Biol. Sci.* **377**, 20210273. doi:10.1098/rstb.2021.0273
Zaccardi, G., Kelber, A., Sison-Mangus, M. P. and Briscoe, A. D. (2006). Color discrimination in the red range with only one long-wavelength sensitive opsin. *J. Exp. Biol.* **209**, 1944-1955. doi:10.1242/jeb.02207
Zeil, J. (1983). Sexual dimorphism in the visual system of flies: the compound eyes and neural superposition in Bibionidae (Diptera). *J. Comp. Physiol. A* **150**, 379-393. doi:10.1007/BF00605027

Zhan, S. and Reppert, S. M. (2012). MonarchBase: the monarch butterfly genome database. *Nucleic Acids Res.* **41**, D758-D763. doi:10.1093/nar/gks1057

Zhao, H., Ru, B., Teeling, E. C., Faulkes, C. G., Zhang, S. and Rossiter, S. J. (2009). Rhodopsin molecular evolution in mammals inhabiting low light environments. *PLoS ONE* **4**, e8326. doi:10.1371/journal.pone.0008326

Ziemba, K. S. and Rutowski, R. L. (2000). Sexual dimorphism in eye morphology in a butterfly (*Asterocampa leilia*; Lepidoptera, Nymphalidae). *Psyche* **103**, 25-36. doi:10.1155/2000/54503

Zufall, F., Schmitt, M. and Menzel, R. (1989). Spectral and polarized light sensitivity of photoreceptors in the compound eye of the cricket (*Gryllus bimaculatus*). *J. Comp. Physiol. A* **164**, 597-608. doi:10.1007/BF00614502